Angewandte Chemie
Eine Zeitschrift der Gesellschaft Deutscher Chemiker

Supporting Information

69451 Weinheim, Germany

Synthesis, Characterization, and Chirality of the N-confused Porphyrin Dimer Zinc Complexes. Toward Enantioselective Synthesis of Bis(porphyrinoid) Systems

Marta Siczek, Piotr J. Chmielewski

^{1}H NMR data for **3**-$(AcO)_2$ (500 MHz, $CDCl_3$, 298 K) δ (TMS) = 8.26 (d, $^3J_{HH}$ = 4.5 Hz, 1H, pyrrole); 8.21 (d, $^3J_{HH}$ = 6.4 Hz, 2H, tolyl); 7.98 (d, $^3J_{HH}$ = 4.4 Hz, 1H, pyrrole); 7.89 (d, $^3J_{HH}$ = 4.6 Hz, 1H, pyrrole); 7.86 (d, $^3J_{HH}$ = 4.5 Hz, 1H, pyrrole); 7.82 (d, $^3J_{HH}$ = 4.4 Hz, 1H, pyrrole); 7.74 (m, 4H, tolyl); 7.57 (b, 2H, tolyl); 7.41 (b, 2H, tolyl); 7.36 (b, 2H, tolyl) ; 7.29 (d, $^3J_{HH}$ = 7.8 Hz, 1H, tolyl); 2.60 (s, 6H, tolyl Me); 2.51 (s, 3H, tolyl Me); 2.50 (s, 3H, tolyl Me); -0.66 (s, 3H, acetate Me); -1.31 (s, 1H, 21).

^{1}H NMR data for **3**-$(AcO)_2$ (500 MHz, $CDCl_3$, 213 K) δ (TMS) = 11.82 (s, 1H, 2-NH) ; 8.37 (d, $^3J_{HH}$ = 7.5 Hz, 1H, tolyl); 8.36 (d, $^3J_{HH}$ = 6.8 Hz, 1H, tolyl); 8.23 (d, $^3J_{HH}$ = 3.4 Hz, 1H, pyrrole); 7.99 (d, $^3J_{HH}$ = 7.2 Hz, 1H, tolyl); 7.90 (d, $^3J_{HH}$ = 3.5 Hz, 1H, pyrrole); 7.86 (m, 4H, tolyl); 7.80 (d, $^3J_{HH}$ = 7.9 Hz, 2H, tolyl); 7.76 (d, $^3J_{HH}$ = 7.0 Hz, 1H, tolyl); 7.68 (d, $^3J_{HH}$ = 3.7 Hz, 1H, tolyl); 7.55 (d, $^3J_{HH}$ = 7.2 Hz, 1H, tolyl); 7.49 (d, $^3J_{HH}$ = 7.5 Hz, 2H, tolyl); 7.36 (d, $^3J_{HH}$ = 7.2 Hz, 1H, tolyl); 7.31 (d, $^3J_{HH}$ = 6.7 Hz, 1H, tolyl); 7.28 (d, $^3J_{HH}$ = 8.0 Hz, 1H, tolyl); 7.15 (d, $^3J_{HH}$ = 6.9 Hz, 1H, tolyl); 2.63 (s, 3H, tolyl Me); 2.58 (s, 6H, tolyl, Me); 2.48 (s, 3H, tolyl, Me); –0.69 (s, 3H, acetate Me); –1.24 (s, 1H, 21).

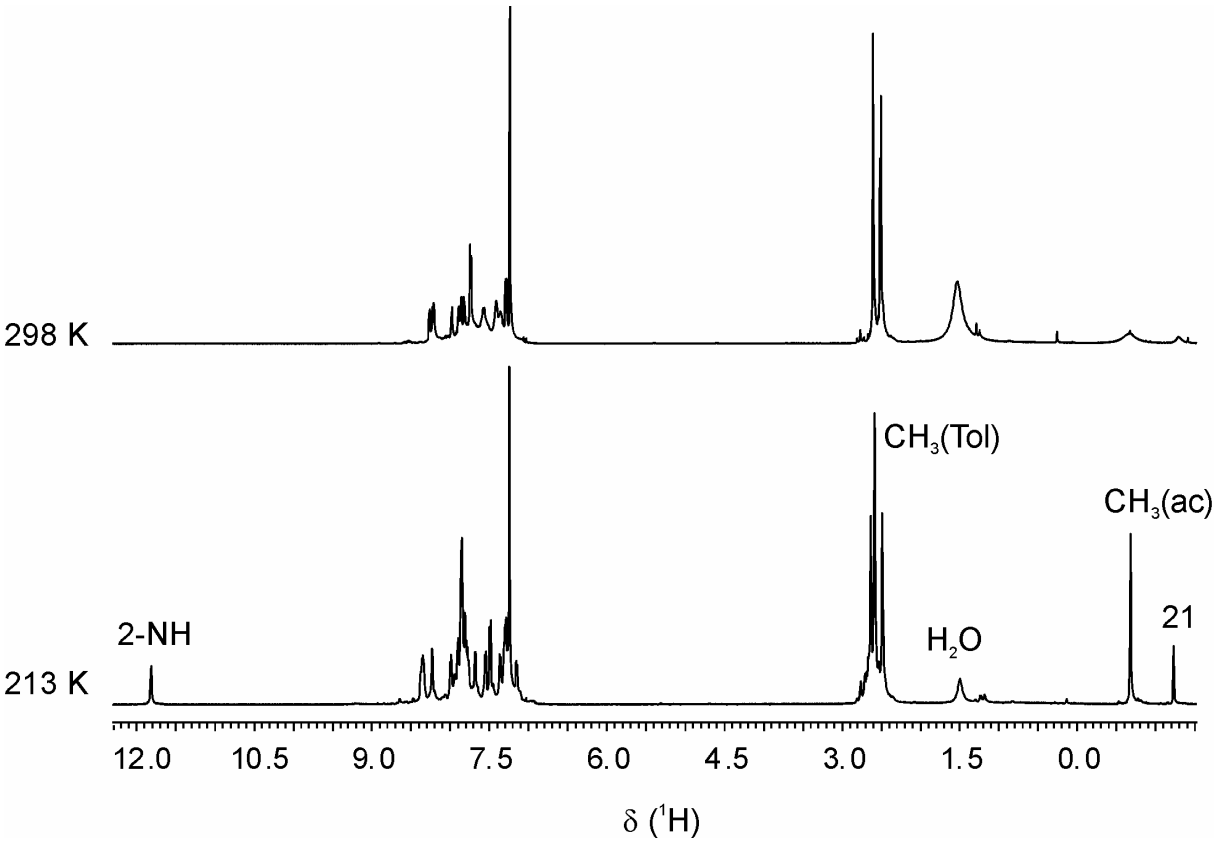

Fig. S1. ^{1}H NMR spectra (500 MHz, $CDCl_3$) recorded at specified temperatures.

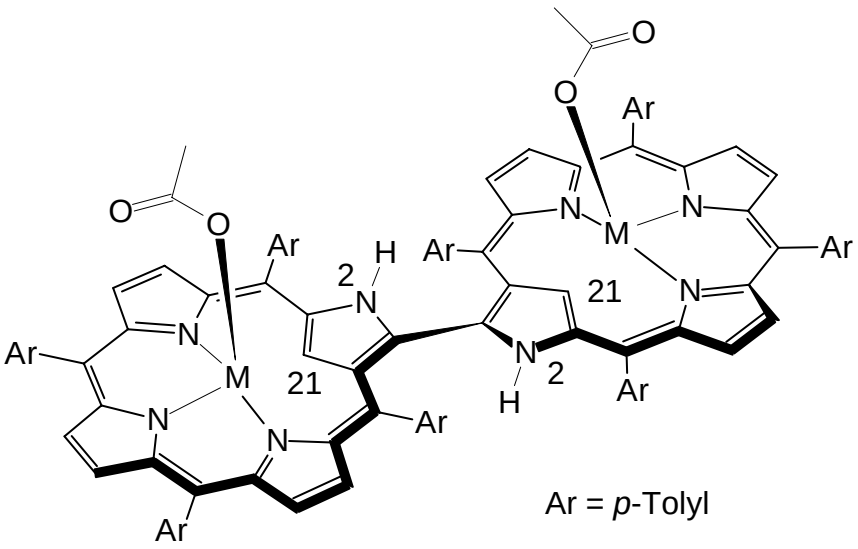

3-$(AcO)_2$

^{1}H NMR data for **3**-Cl_2 (500 MHz, $CDCl_3$, 298 K) δ (TMS) = 9.84 (b, 1H, 2-NH); 8.16 (d, $^{3}J_{HH}$ = 5.0 Hz, 1H, pyrrole);7.9 (d, $^{3}J_{HH}$ = 5.0 Hz, 1H, pyrrole);7.85 (d, $^{3}J_{HH}$ = 7.3 Hz, 2H, tolyl);7.84 (d, $^{3}J_{HH}$ = 4.8 Hz, 1H, pyrrole); 7.75 (d, $^{3}J_{HH}$ = 4.8 Hz, 1H, pyrrole);7.72 (d, $^{3}J_{HH}$ = 4.8 Hz, 1H, poyrrole); 7.63 (d, $^{3}J_{HH}$ = 4.8 Hz, 1H, pyrrole); 7.59 (d, $^{3}J_{HH}$ = 8.0 Hz, 2H, tolyl); 7.55 (b, 2H, tolyl); 7.49 (b, 2H, tolyl); 7.40 (b, 2H, tolyl); 7.30 (b, 1H, tolyl); 7.28 (d, 8.2 Hz, 2H, tolyl); 2.59 (s, 3H, tolyl Me); 2.56 (s, 3H, tolyl Me); 2.53 (s, 3H, tolyl Me); 2.49 (s, 3H, tolyl Me); 1.44 (b, H_2O); -0.71 (s, $^{4}J_{HH}$ = 1.0 Hz, 1H, 21).

^{1}H NMR data for **3**-Cl_2 (500 MHz, $CDCl_3$, 213 K) δ (TMS) = 10.51 (b, 1H, 2-NH); 8.20 (d, $^{3}J_{HH}$ = 5.0 Hz, 1H, 7); 8.02 (b, 1H, tolyl); 7.92 (d, $^{3}J_{HH}$ = 4.8 Hz, 1H, 18); 7.8 (d, $^{3}J_{HH}$ = 7.8 Hz, 1H, 5*o*); 7.84 (d, $^{3}J_{HH}$ = 4.8 Hz, 1H, 8); 7.79 (d, $^{3}J_{HH}$ = 4.8 Hz, 1H, 12); 7.77 (d, $^{3}J_{HH}$ = 4.8 Hz, 1H, 13); 7.74 (b, 2H, 20*o'*, 20*m*'); 7.72 (b, 2H, tolyl, *m*); 7.60 (d, $^{3}J_{HH}$ = 4.6 Hz, 1H, 17); 7.55 (d, $^{3}J_{HH}$ = 7.3 Hz, 1H, 10*o*); 7.51 (d, $^{3}J_{HH}$ = 6.6 Hz, 1H, 15*o*); 7.49 (d, $^{3}J_{HH}$ = 6.7 Hz, 1H, 15*o*'); 7.44 (d, 7.3 Hz, 1H, tolyl, *m*); 7.36 (d, $^{3}J_{HH}$ = 7.3 Hz, 1H, 10*m*); 7.32 (d, $^{3}J_{HH}$ = 7.1 Hz, 1H, 20*o*); 7.28 (d, $^{3}J_{HH}$ = 9.2 Hz, 2H, 15*m*); 7.03 (d, $^{3}J_{HH}$ = 6.9 Hz, 1H, 20*m*); 2.60 (s, 3H, tolyl Me); 2.60 (s, 3H, tolyl Me); 2.57 (s, 3H, tolyl Me); 2.47 (s, 3H, tolyl Me); 0.91 (s, 2H, H_2O); -0.90 (s, 1H, 21)

^{13}C NMR data for **3**-Cl_2 (126 MHz, $CDCl_3$, 298 K) δ (TMS) = 161.8; 156.9; 156.8; 152.4; 152.0; 138.9; 138.6; 138.4; 138.2; 137.5; 137.0; 136.8; 136.1; 135.0; 134.6; 134.3; 133.4; 133.0; 132.4; 131.5; 129.2; 128.5; 127.8; 117.3; 117.2; 115.0; 75.4 (*C*21); 21.6; 21.4; 21.3.

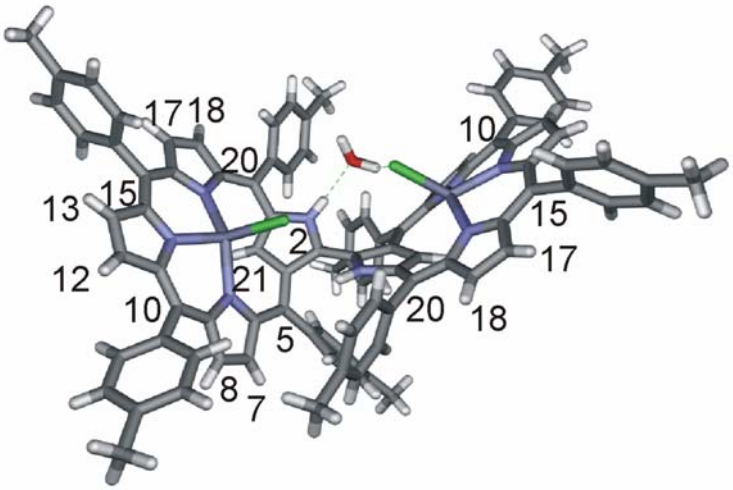

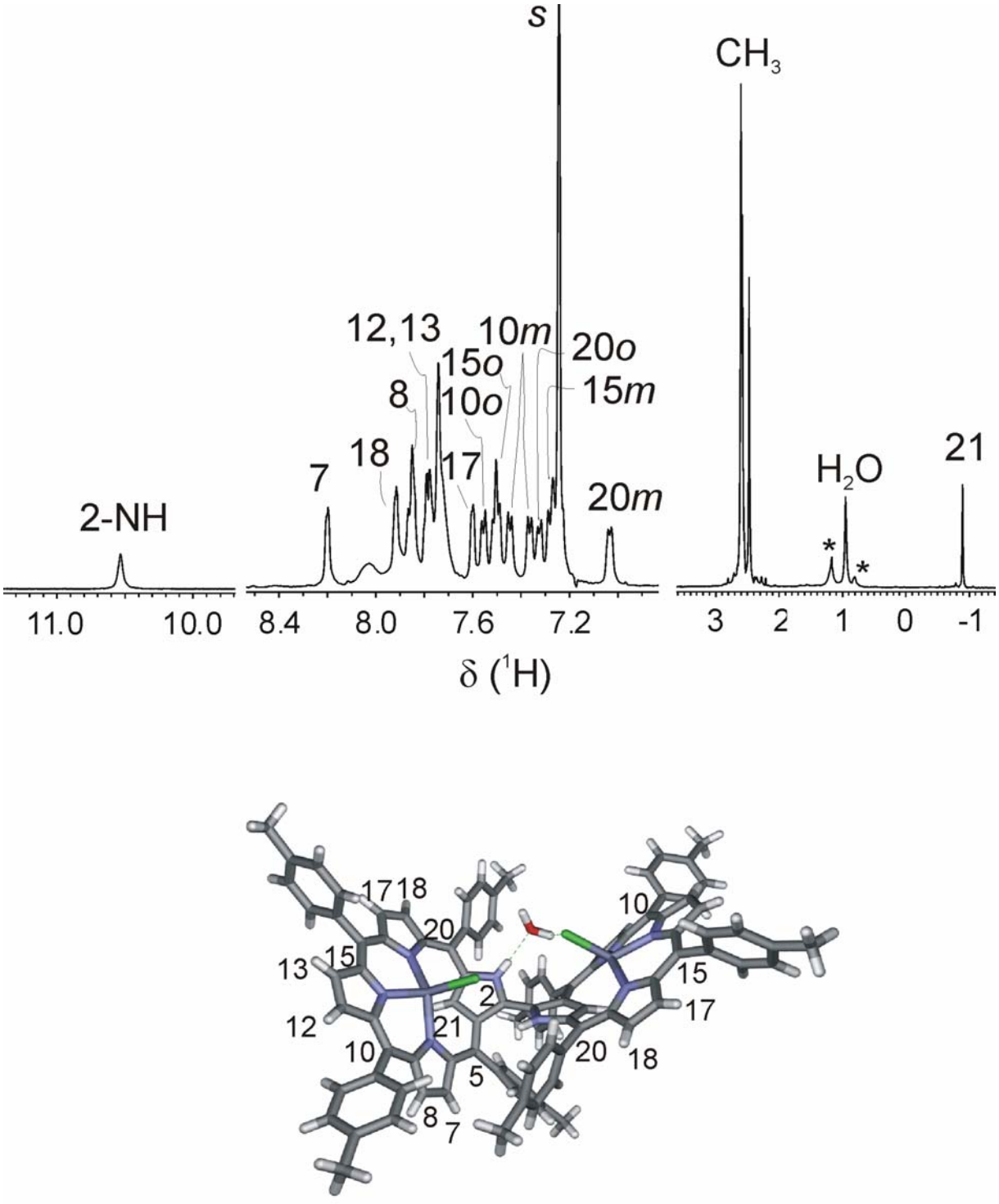

Fig. S2. ^{1}H NMR spectrum (500 MHz, $CDCl_3$, 213 K) of **3**-Cl_2 and wire-frame representation of its molecular structure. Proton signal assignments in the spectrum follow these in the model, *s* - solvent.

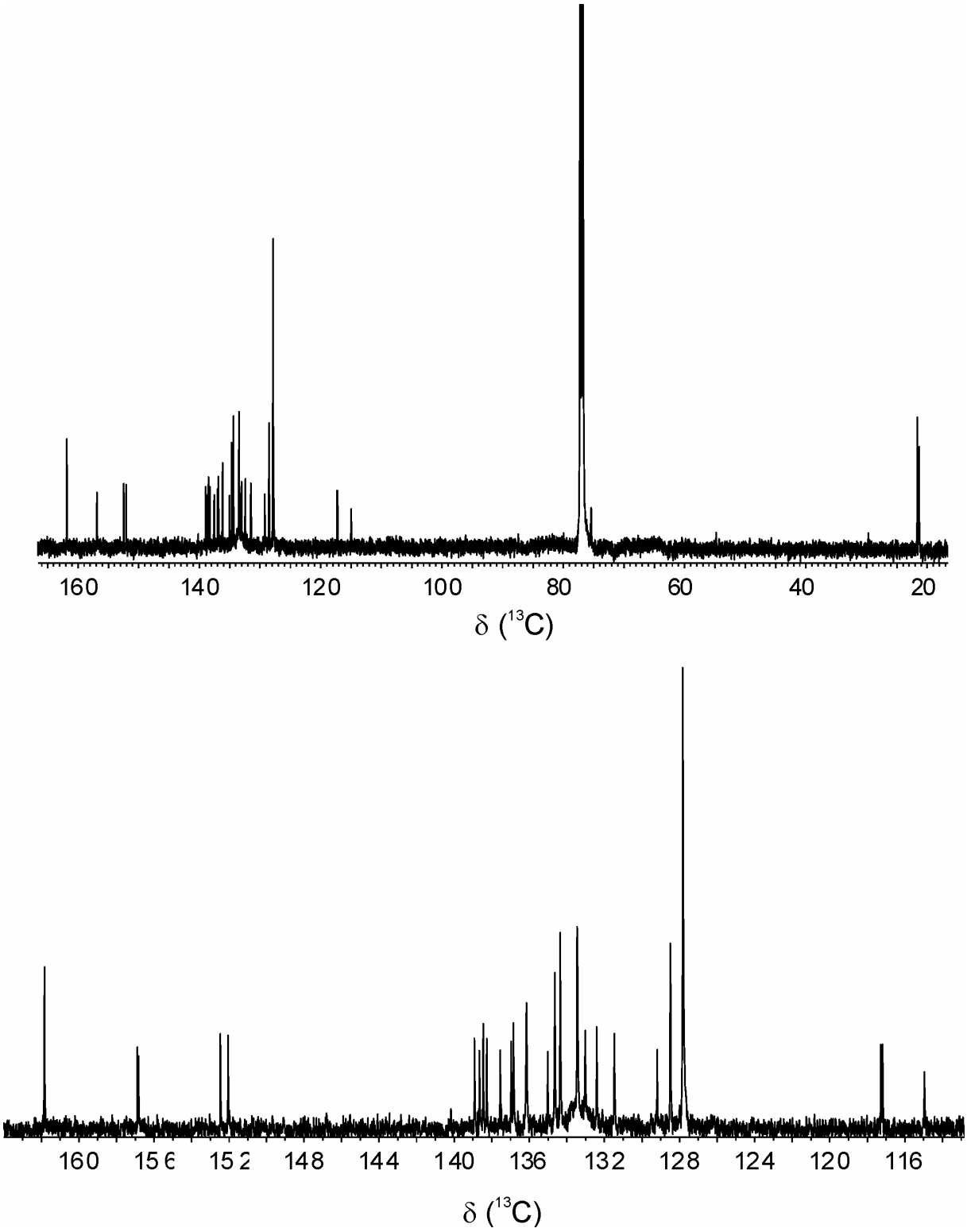

Fig. S3. ^{13}C NMR spectrum (126 MHz, $CDCl_3$, 298 K) of **3**-Cl_2.

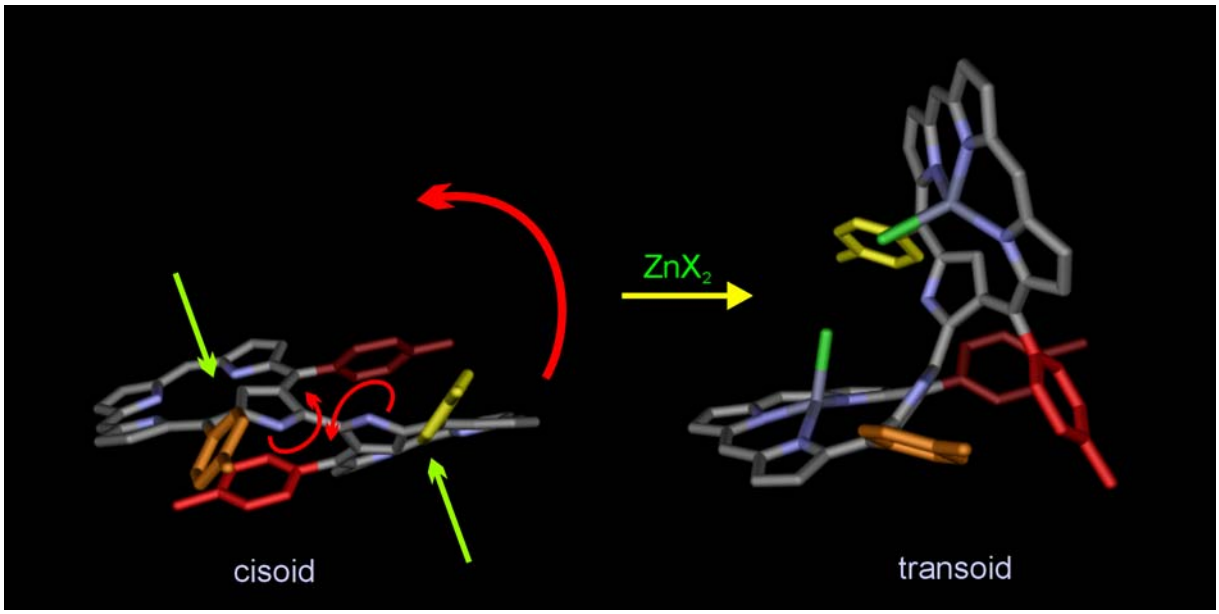

Fig. S4. Intramolecular alteration of ligand structure of **2** upon zinc insertion with concurrent cisoid-transoid transformation of the bipyrrole moiety leading to the formation of **3**-Cl_2. The incoming metal ions are symbolized by green arrows, the bent thin red arrows indicate rotation of N-confused pyrroles around 3,3'-bond, and the thick red arrow shows direction of the resulting shift of one of the subunits while the other subunit is kept motionless. Only 5- and 20-tolyl substituents are shown for both subunits in the wire-frame representations of molecular structures of **2** (left) and **3**-Cl_2 (right).

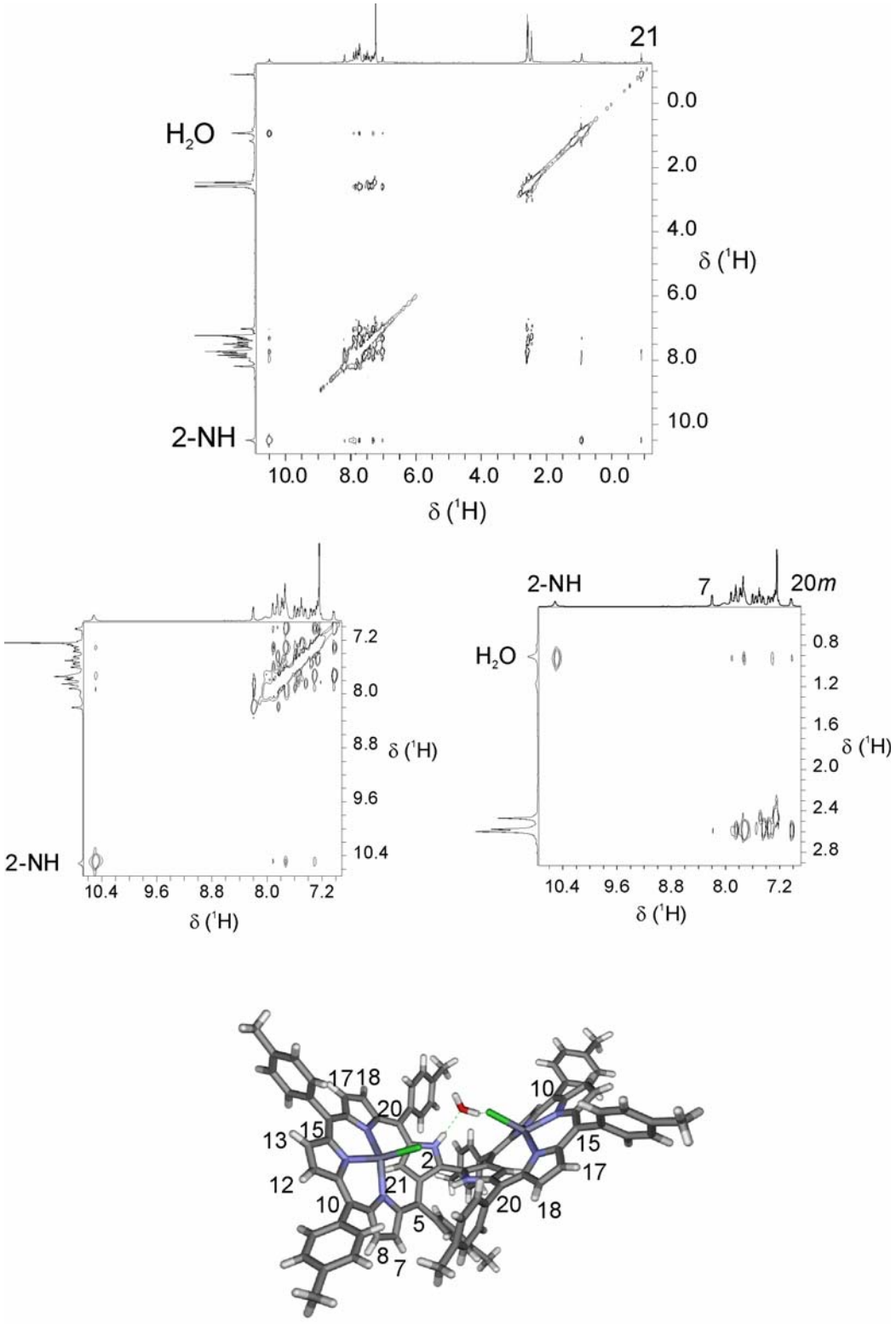

Fig. S5. NOESY spectrum ($CDCl_3$, 213K) of **3**-Cl_2 (upper map) and its fragments (lower maps) showing details of through-space interactions of 2-NH and water bound inside the dimeric complex.

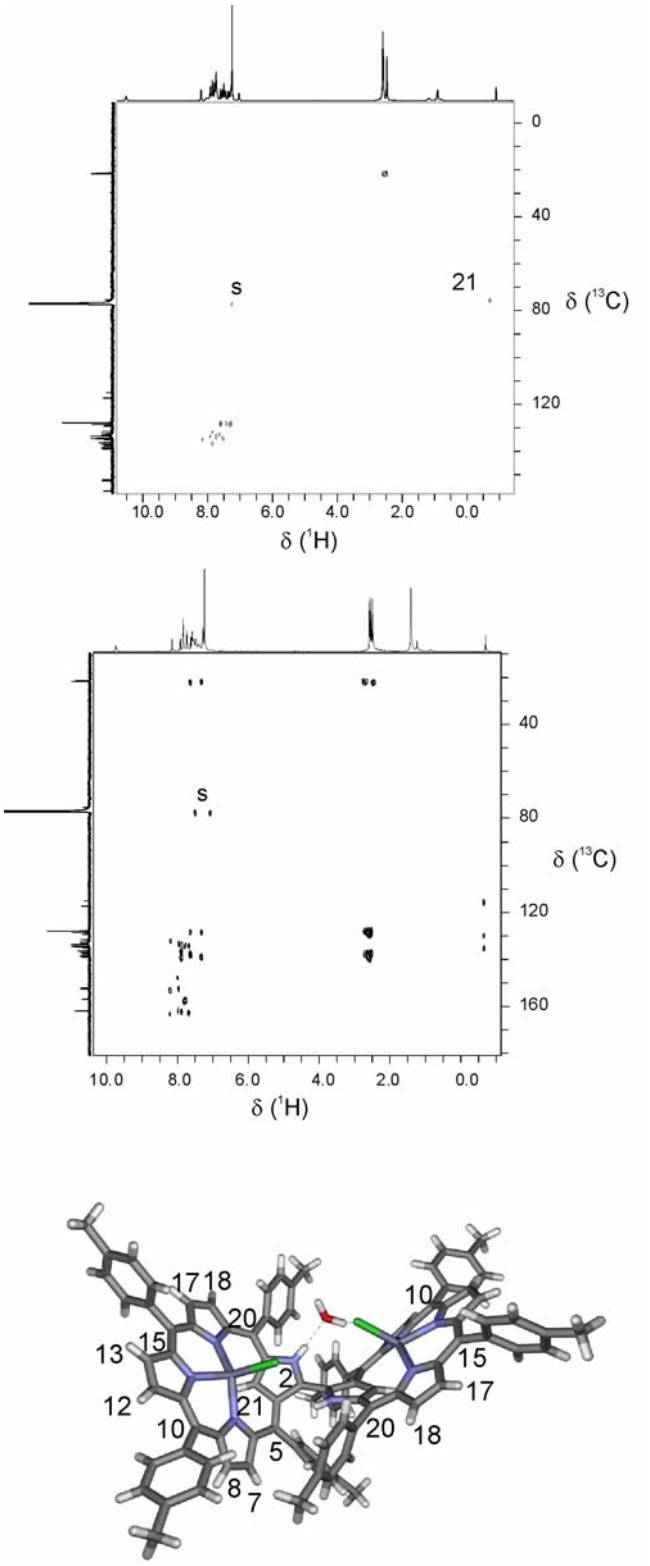

Fig. S6. ^{1}H-^{13}C HMQC ($CDCl_3$, 213 K, upper map) and ^{1}H-^{13}C HMBC ($CDCl_3$, 213 K, lower map) of **3**-Cl_2.

^{1}H NMR data for **3**-tart (500 MHz, $CDCl_3$, 298 K) δ (TMS) = 9.15 (s, 1H, 2-NH); 8.23 (d, $^{3}J_{HH}$ = 4.9 Hz, 1H, pyrrole); 7.87 (d, $^{3}J_{HH}$ = 8.0 Hz, 2H, tolyl); 7.79 (d, $^{3}J_{HH}$ = 4.9 Hz, 1H, pyrrole); 7.74 (d, $^{3}J_{HH}$ = 8.0 Hz, 2H, tolyl); 7.68 (d, $^{3}J_{HH}$ = 5.1 Hz, 1H, pyrrole); 7.67 (d, $^{3}J_{HH}$ = 4.9 Hz, 1H, pyrrole); 7.61 (d, $^{3}J_{HH}$ = 7.8 Hz, 1H, tolyl); 7.59 (d, $^{3}J_{HH}$ = 4.9 Hz, 1H, pyrrole); 7.52 (d, $^{3}J_{HH}$ = 4.7 Hz, 1H, pyrrole); 7.51 (b, 1H, tolyl); 7.40 (d, $^{3}J_{HH}$ = 6.9 Hz, 2H, tolyl); 2.69 (s, 3H, tolyl Me); 2.66 (s, 3H, tolyl Me); 2.58 (s, 3H tolyl Me); 2.46 (s, 3H tolyl Me); 1.83 (m, AA'XX', 1H, tartarate CH); 1.43 (m, AA'XX', 1H, tartarate OH); -0.58 (d, $^{4}J_{HH}$ = 1.0 Hz, 1H, 21).

^{1}H NMR data for **3**-tart (500 MHz, $CDCl_3$, 213 K) δ (TMS) = 9.15 (s, 1H, 2-NH); 8.21 (d, $^{3}J_{HH}$ = 4.6 Hz, 1H, 7); 7.96 (d, $^{3}J_{HH}$ = 6.9 Hz, 2H, 5*o*, 10*o*); 7.85 (d, $^{3}J_{HH}$ = 8.0 Hz, 2H, 10*o*',10*m*); 7.83 (d, $^{3}J_{HH}$ = 6.9 Hz, 1H, 20*m'*); 7.79 (d, $^{3}J_{HH}$ = 4.5 Hz, 1H, 18); 7.74 (d, $^{3}J_{HH}$ = 6.7 Hz, 1H, 20*o'*); 7.68 (d, $^{3}J_{HH}$ = 5.0 Hz, 1H, 8); 7.67 (d, $^{3}J_{HH}$ = 6.2 Hz, 2H, 15*o*); 7.61 (d, $^{3}J_{HH}$ = 4.3 Hz, 1H, 12); 7.49 (d, $^{3}J_{HH}$ = 4.3 Hz, 1H, 13); 7.48 (d, $^{3}J_{HH}$ = 8.0 Hz, 2H, 5*m*, 5*o'*); 7.42 (d, $^{3}J_{HH}$ = 7.1 Hz, 1H, 20*o*); 7.36 (d, $^{3}J_{HH}$ = 8.0 Hz, 1H, 15*o'*); 7.32 (d, $^{3}J_{HH}$ = 7.3 Hz, 2H, 5*m'*, 20*m*); 7.28 (d, $^{3}J_{HH}$ = 8.3 Hz, 1H, 15*m*); 7.21 (d, $^{3}J_{HH}$ = 6.6 Hz, 1H, 15*m'*); 2.70 (s, 3H, tolyl Me); 2.67 (s, 3H, tolyl Me); 2.56 (s, 3H, tolyl Me); 2.44 (s, 3H, tolyl Me); 1.80 (m, 1H, tartarate CH); 1.54 (m, 1H, tartarate OH); -0.67 (s, 1H, 21).

^{13}C NMR data for **3**-tart (126 MHz, $CDCl_3$, 298 K) δ (TMS) = 173.0 (*C*=O, tartarate); 162.6; 162.2; 156.9; 156.7; 152.4; 152.2; 139.1; 138.9; 138.5; 138.0; 137.4; 136.9; 136.8; 136.7; 136.3; 135.2; 135.1; 134.1; 133.5; 133.3; 133.2; 132.9; 132.1; 131.8; 130.6; 128.7; 128.2; 128.1; 127.8; 127.7; 127.6; 116.8; 116.6; 111.9; 69.4 (21-*C*H); 68.5 (*C*H tartarate); 21.8; 21.8; 21.4; 21.3

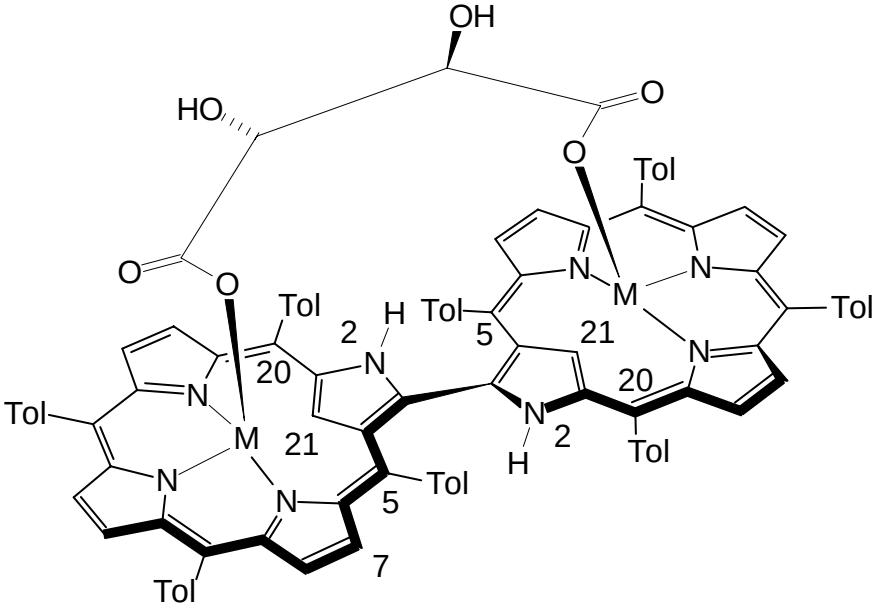

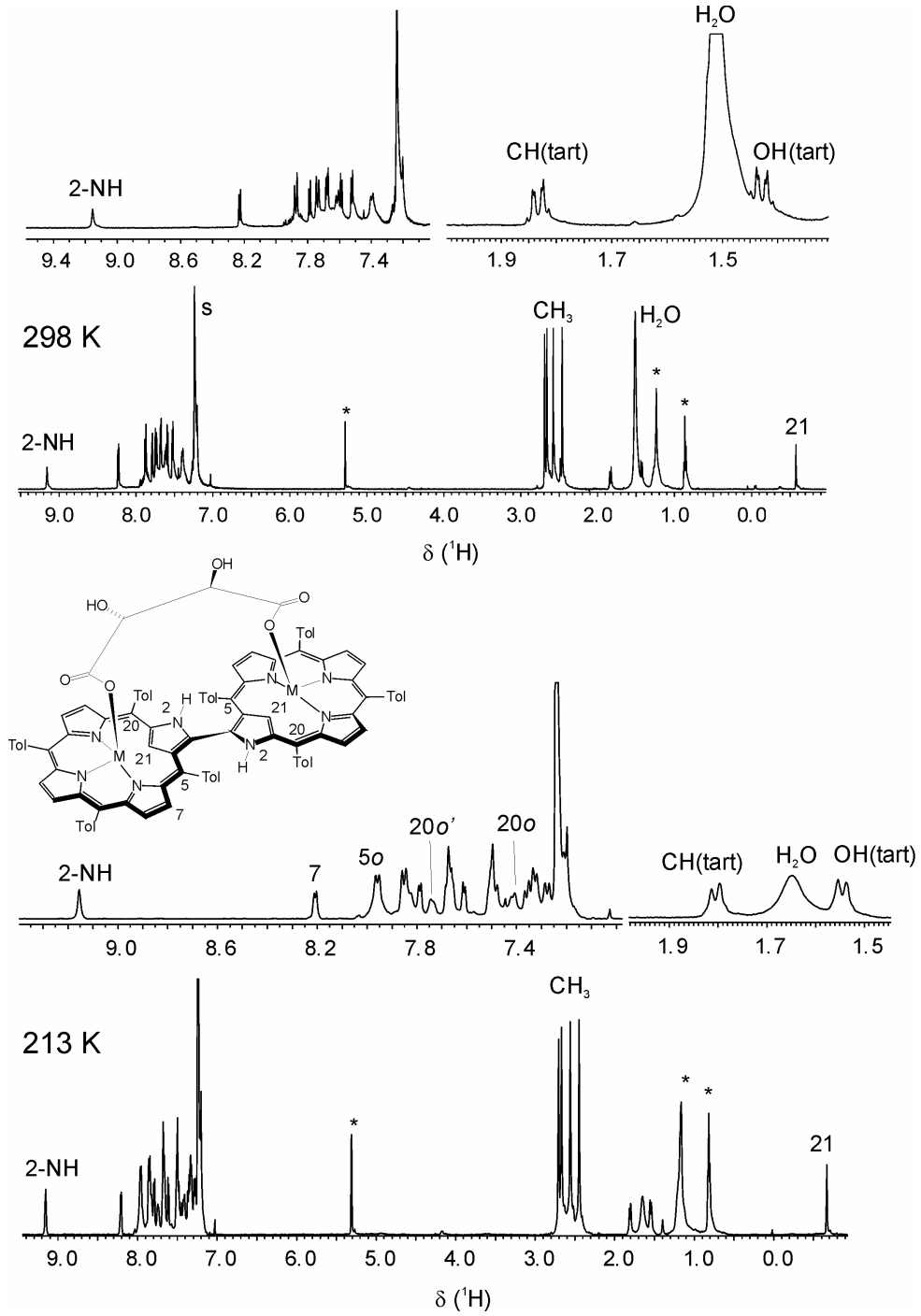

Fig. S7. ^{1}H NMR spectra (500 MHz, $CDCl_3$) of **3**-tart, upper traces at 298 K, lower traces at 213 K. The impurity signals are marked with asterisk.

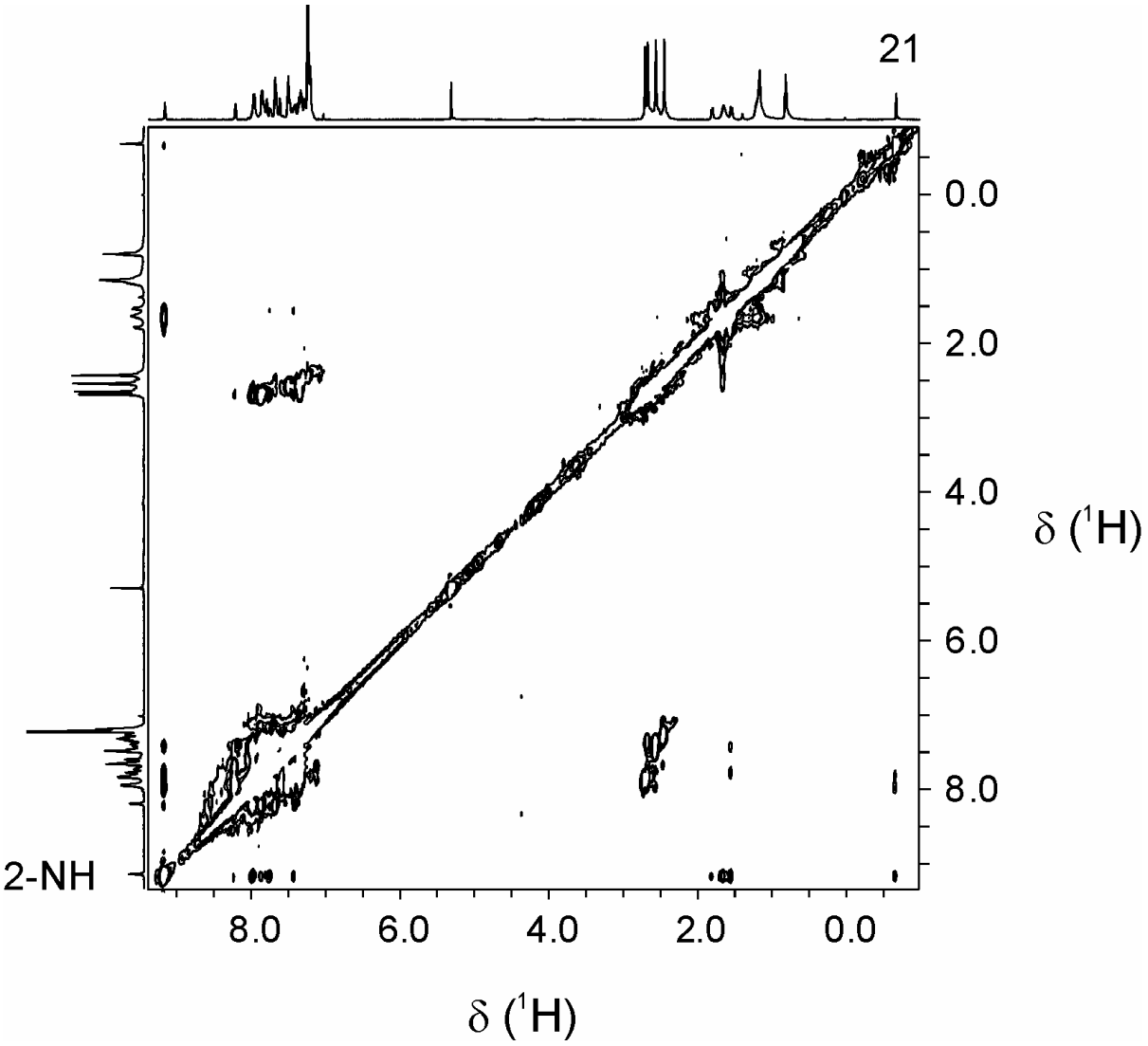

Fig. S8. NOESY spectrum ($CDCl_3$, 213K) of **3**-tart.

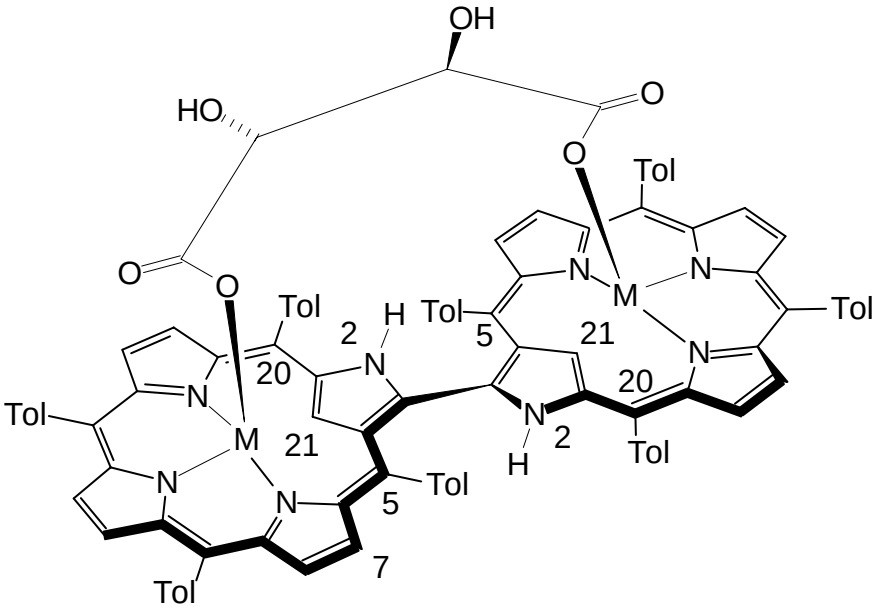

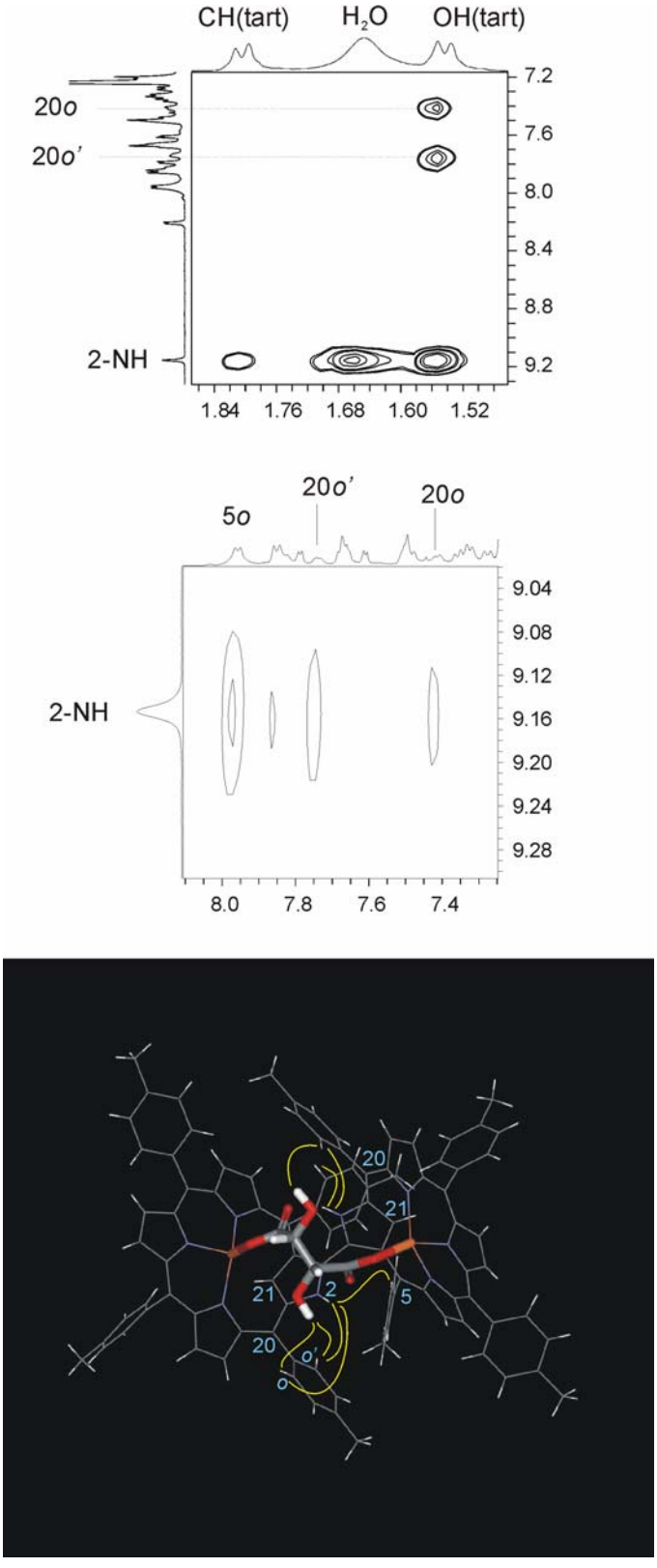

Fig. S9. Fragments of the NOESY spectrum of **3**-tart ($CDCl_3$, 213 K) showing through-space interaction of tartarate and macrobicyclic ligand protons. These interprotonic contacts are depicted in a form of yellow curves superimposed on the energy-optimized model of the *M-R,R* diastereomer.

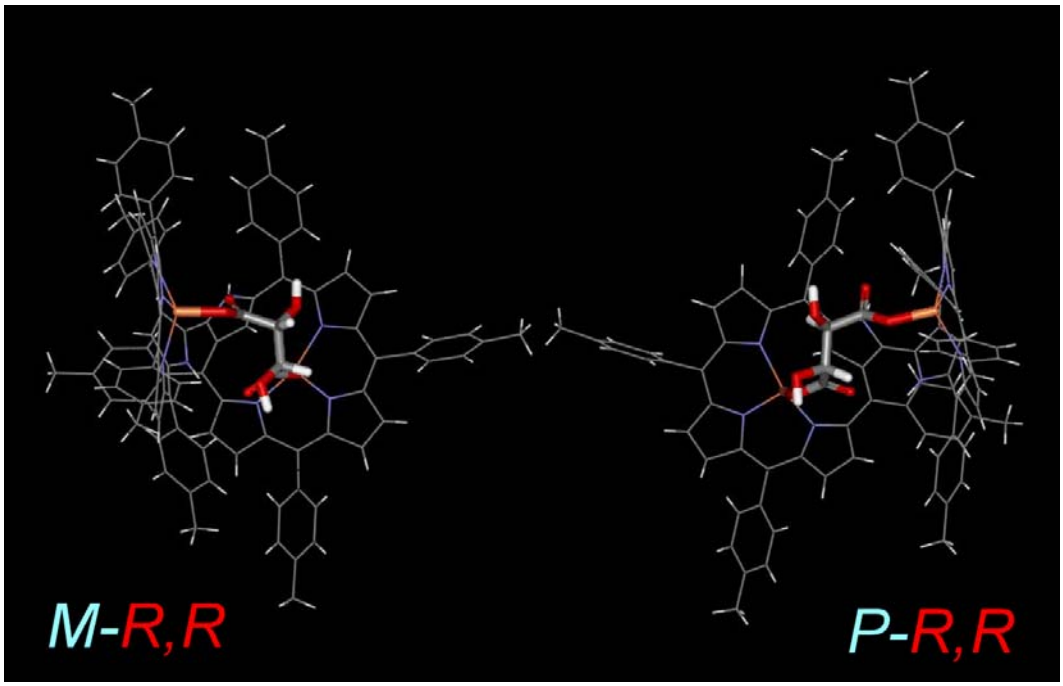

Fig. S10. The energy-optimized models of possible diastereomers of **3**-(*R,R*)tart. Orientation of the substituents on the asymmetric tartarate carbons in *P-R,R* diastereomer should result in a strong trough-space (NOE) interaction of CH with *meso*-aryl protons (shortest interprotonic distance 2.3 Å) and lack of such interaction for OH. For the *M-R,R* diastereomer no interaction between tartarate CH and macrobicyclic ligand is anticipated (interprotonic distances > 4 Å), while strong NOE should appear between tartarate OH and ortho-protons of the tolyl substituent in the position 20 (shortest distance 2.8 Å).
The models were optimized by PM3 semiempirical method (HyperChem 6.01, Hypercube Inc.). The crystal structure of **3**-Cl_2 with chloride ligands substituted by *R,R*-tartarate was taken as a starting point for the calculations. The total energy of the optimized models is about 8 kcal/mol lower in the case of *M-R,R* diastereomer than that of *P-R,R*.

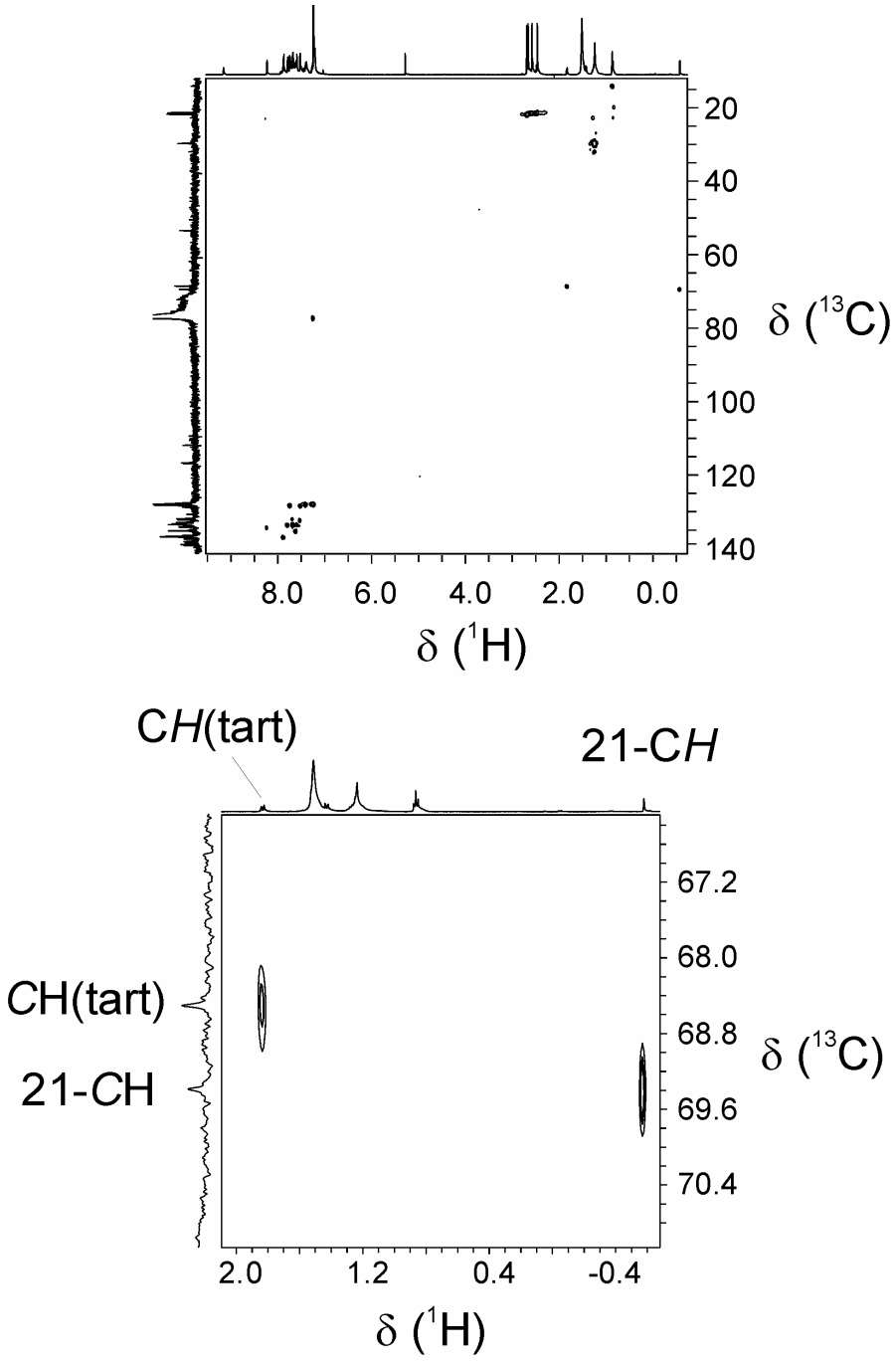

Fig. S11. ^{1}H-^{13}C HMQC of **3**-tart ($CDCl_3$, 298 K, upper map) and its extended fragment (lower map) showing position of tartarate CH and 21-CH signals.

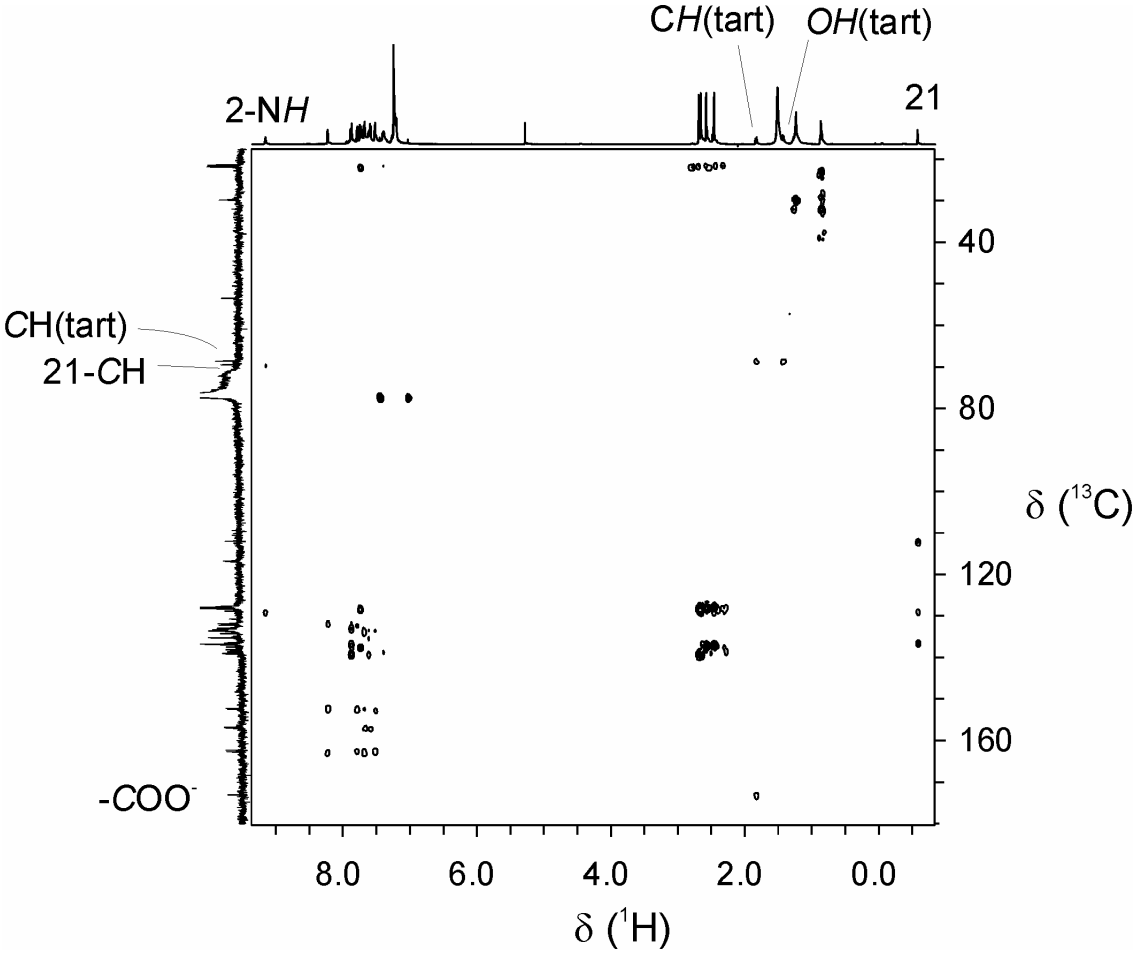

Fig. S12. ^{1}H-^{13}C HMBC of **3**-tart ($CDCl_3$, 298 K).

^{1}H NMR data for **3**-mal (500 MHz, $CDCl_3$, 298 K) δ (TMS) = 10.20 (s, 1H, 2-NH); 9.58 (s, 1H, 26-NH) ; 8.26 (d, $^{3}J_{HH}$ = 5.0 Hz, 1H, pyrrole); 8.23 (d, $^{3}J_{HH}$ = 5.0 Hz, 1H, pyrrole); 8.02 (d, $^{3}J_{HH}$ = 7.8 Hz, 1H, tolyl); 7.89 (d, $^{3}J_{HH}$ = 7.8 Hz, 1H, tolyl); 7.82 (d, $^{3}J_{HH}$ = 4.6 Hz, 1H, pyrrole); 7.81 (d, $^{3}J_{HH}$ = 5.0 Hz, 1H, pyrrole); 7.77 (d, $^{3}J_{HH}$ = 7.3 Hz, 2H, tolyl); 7.74 (d, $^{3}J_{HH}$ = 4.2 Hz, 1H, pyrrole); 7.73 (d, $^{3}J_{HH}$ = 4.2 Hz, 1H, pyrrole); 7.71 (d, $^{3}J_{HH}$ = 5.5 Hz, 1H, tolyl); 7.67 (d, $^{3}J_{HH}$ = 5.5 Hz, 2H, tolyl); 7.64 (d, $^{3}J_{HH}$ = 5.0 Hz, 1H, pyrrole); 7.60 (d, $^{3}J_{HH}$ = 5.0 Hz, 2H, pyrrole); 7.52 (d, $^{3}J_{HH}$ = 5.0 Hz, 1H, pyrrole); 7.50 (b, 2H, tolyl); 7.40 (d, $^{3}J_{HH}$ = 8.3 Hz, 2H, tolyl); 7.38 (b, 1H, tolyl); 7.29 (d, $^{3}J_{HH}$ = 7.8 Hz, 1H, tolyl); 2.67 (s, 6H, tolyl Me); 2.66 (s, 3H, tolyl Me); 2.63 (s, 3H, tolyl Me); 2.58(s, 3H, tolyl Me); 2.57(s, 3H, tolyl, Me); 2.47 (s, 3H, tolyl Me); 2.46 (s, 3H, tolyl Me); 2.17 (d, $^{3}J_{HH}$ = 8.2 Hz, 1H, OH malate); 1.79 (dd, $^{3}J_{HH}$ = 9.7 Hz, $^{3}J_{HH}$ = 8.5 Hz, 1H, 2'-CH malate); 0.43 (dd, $^{2}J_{HH}$ = 13.8 Hz, $^{3}J_{HH}$ = 8.7 Hz, 1H, diastereotopic 3'-CH_2 malate); -0.42 (d, $^{2}J_{HH}$ = 13.8 Hz, 1H, diastereotopic 3'-CH_2 malate); -0.60 (s, 1H, 21); -0.74 (s, 1H, 45).

^{13}C NMR data for **3**-mal (126 MHz, $CDCl_3$, 298 K) δ (TMS) = 175.4; 173.6; 162.5; 162.3; 162.3; 161.6; 156.9; 156.8; 156.7; 156.5; 152.4; 152.3; 152.2; 139.1; 139.0; 139.0; 138.7; 138.6; 138.4; 138.1; 137.7; 137.4; 136.9; 136.8; 136.8; 136.7; 136.7; 136.5; 135.5; 135.4; 135.3; 135.0; 134.5; 134.3; 133.7; 133.6; 133.4; 133.3; 133.2; 133.1; 133.0; 132.5; 132.0; 131.9; 131.6; 131.4; 130.8; 129.7; 129.1; 128.9; 128.2; 128.0; 127.9; 127.8; 127.8; 127.7; 127.6; 116.9; 116.7; 116.7; 116.6; 114.6; 111.7; 72.0; 70.3; 65.7; 37.2; 21.8; 21.7; 21.7; 21.4; 21.3

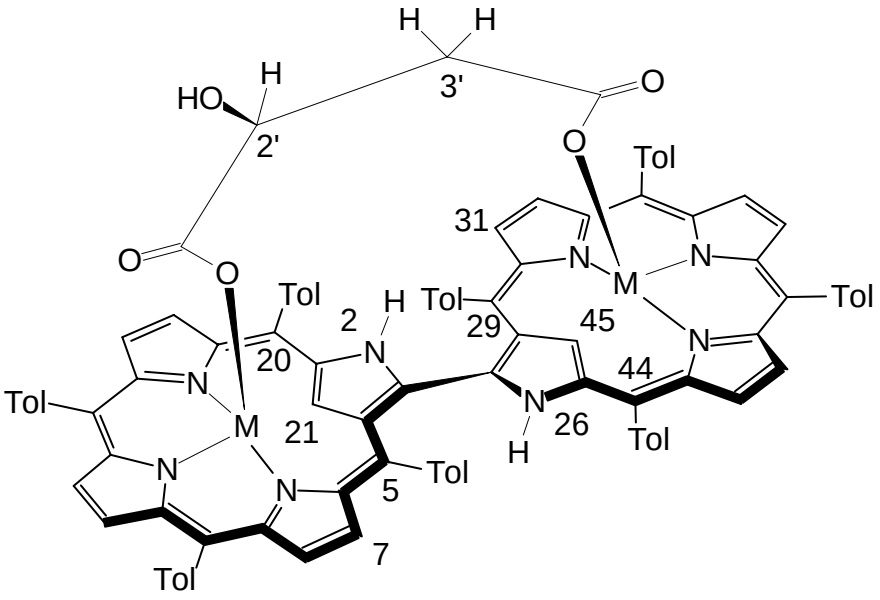

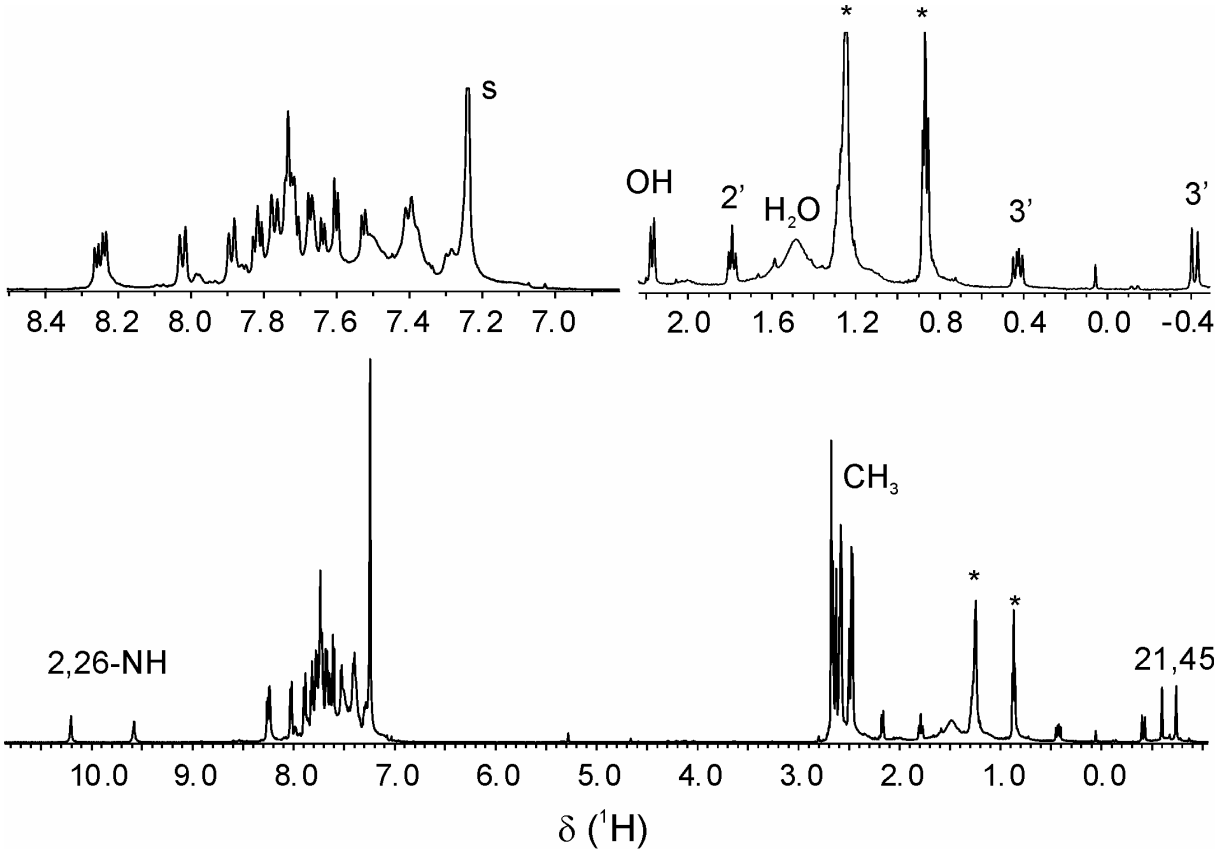

Fig. S13. ^{1}H NMR spectra (500 MHz, 298 K, $CDCl_3$) of **3**-mal. The impurity signals are marked with asterisk.

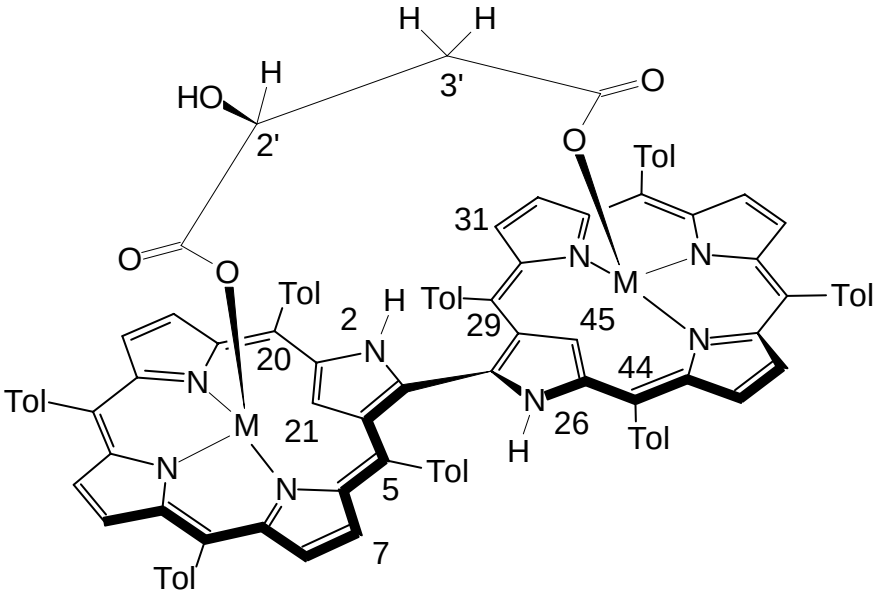

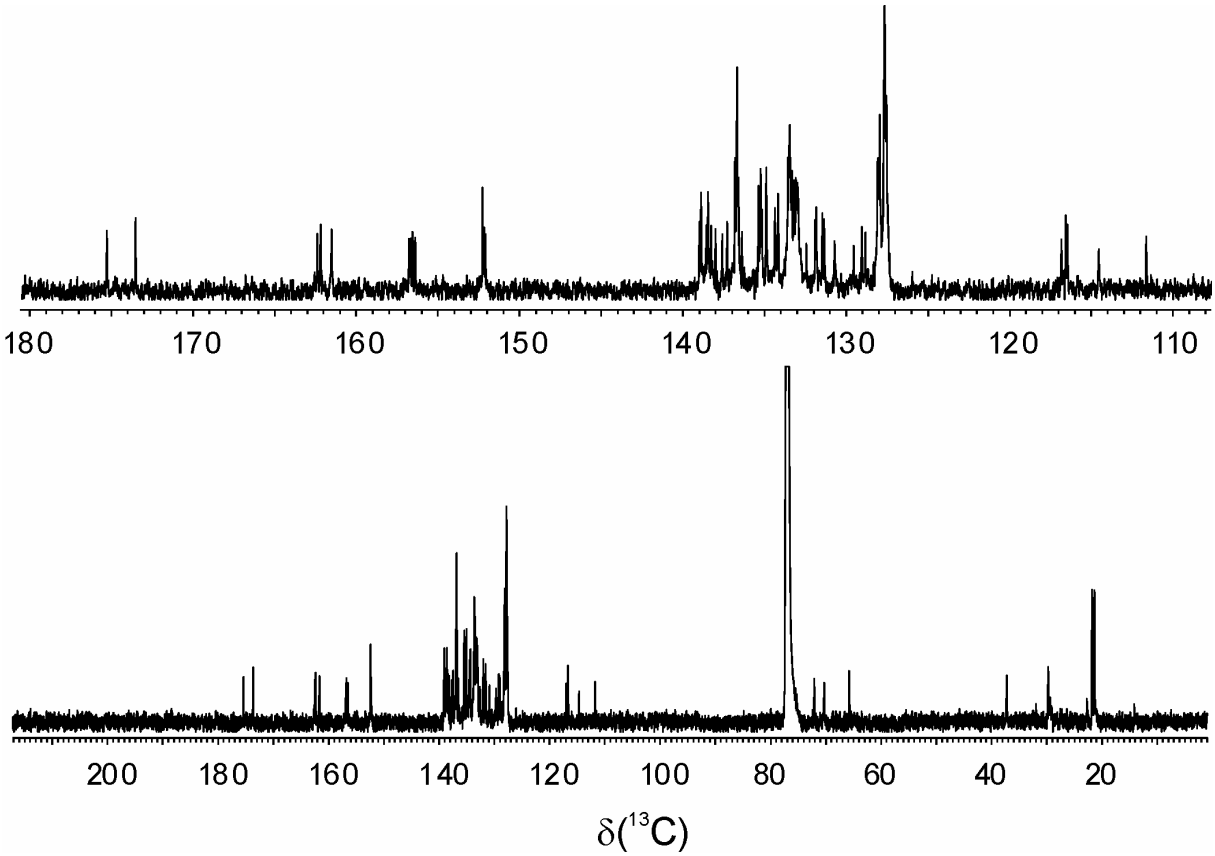

Fig. S14. ^{13}C NMR spectra (126 MHz, 298 K, $CDCl_3$) of **3**-mal.

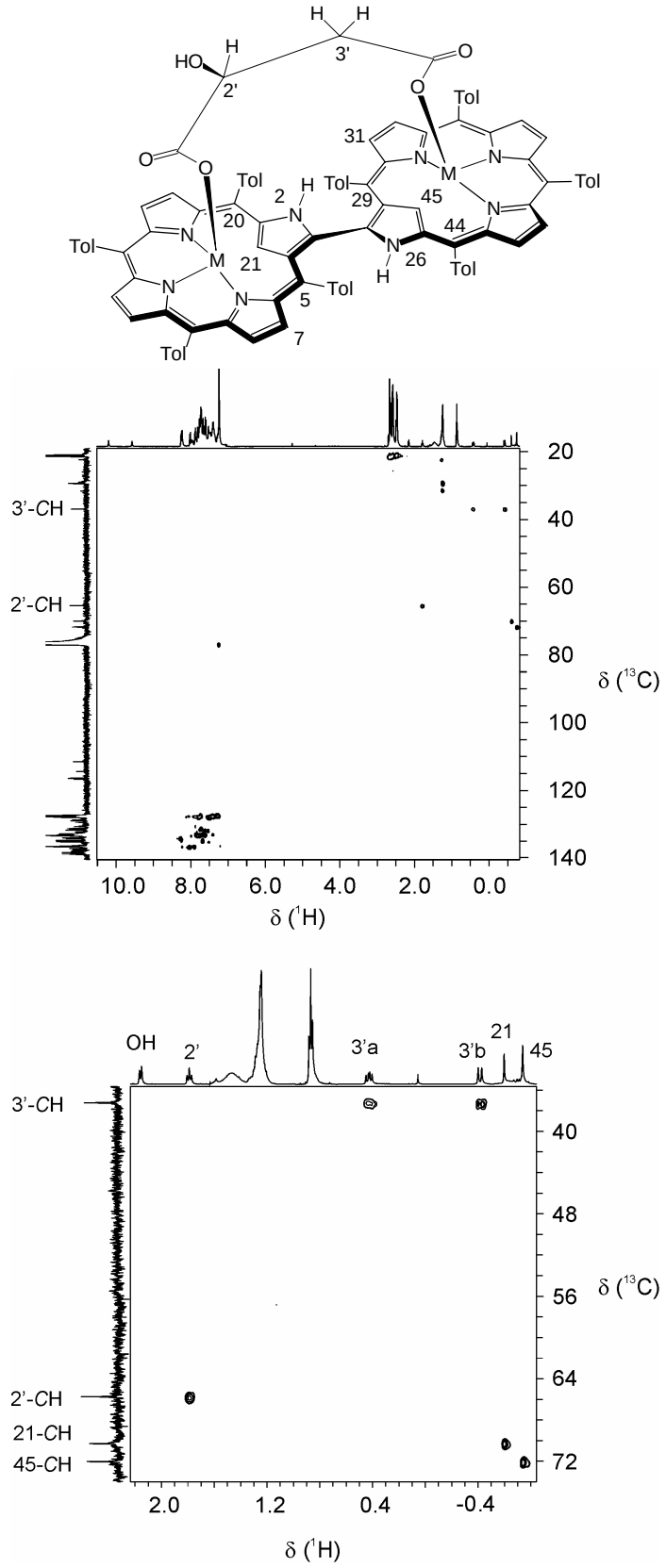

Fig. S15. ^{1}H-^{13}C HMQC of **3**-mal ($CDCl_3$, 298 K, upper map) and its extended fragment (lower map) showing position of malate 2'-CH and 21,45-CH signals.

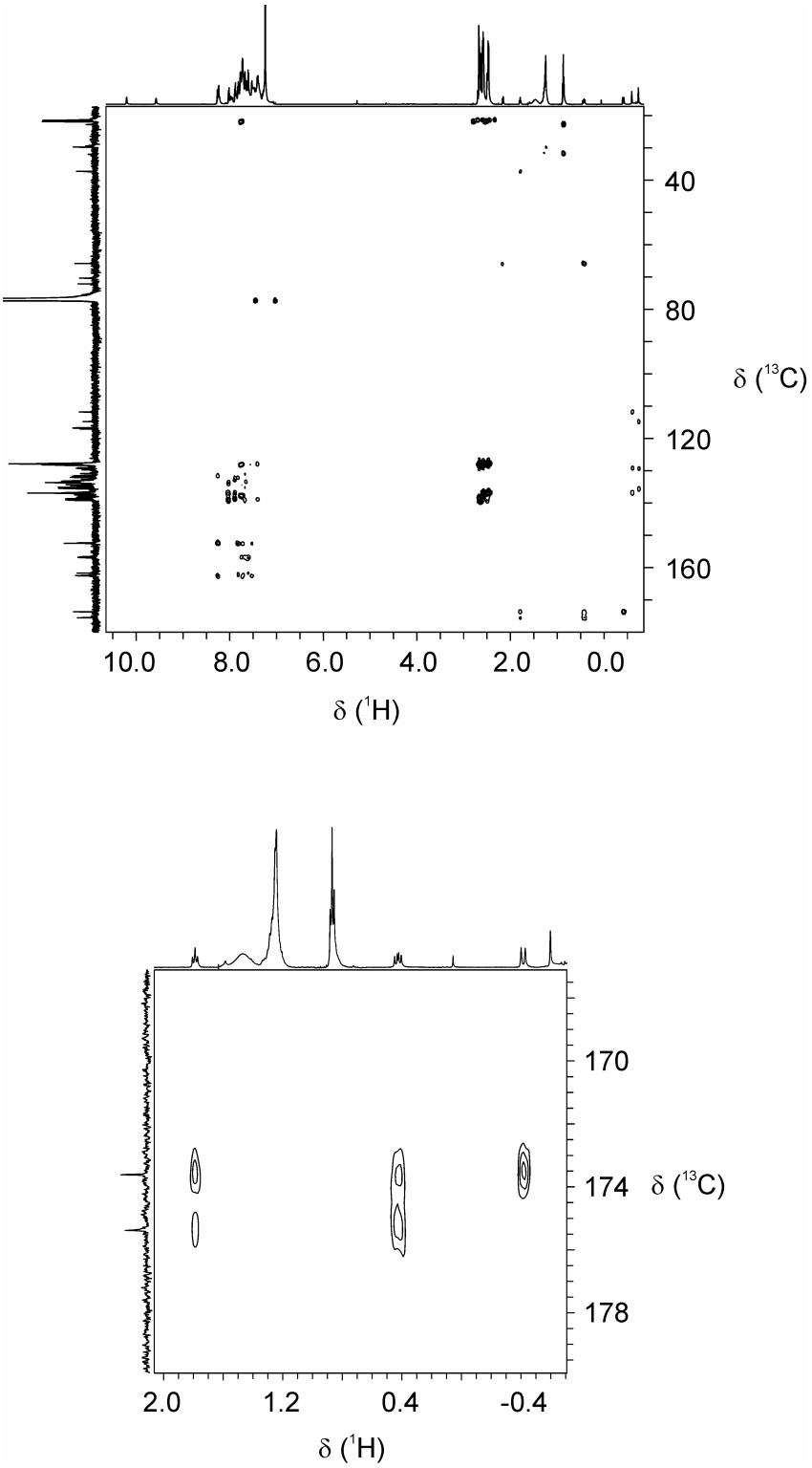

Fig. S16. ^{1}H-^{13}C HMBC of **3**-mal ($CDCl_3$, 298 K, upper map) and its extended fragment (lower map) showing position of malate *C*=O signals.

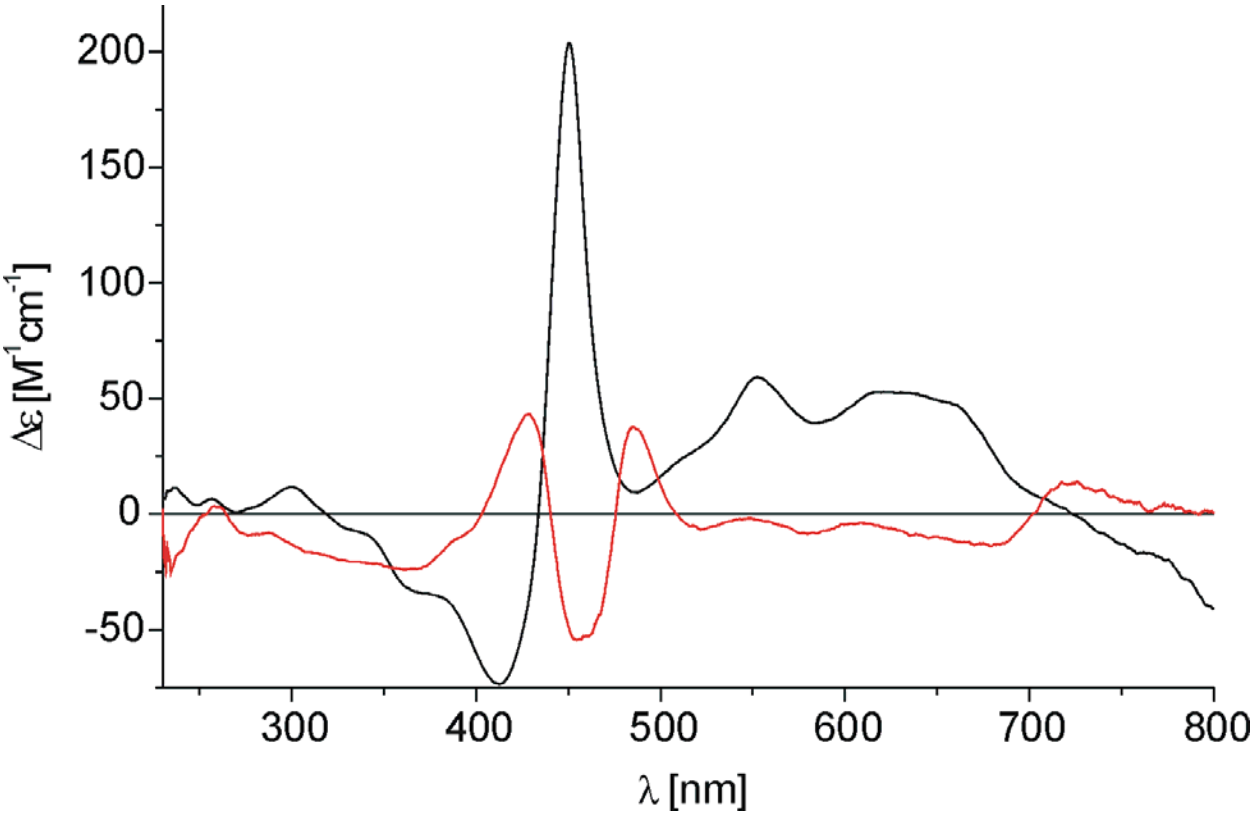

Fig. S17. CD spectra of CH_2Cl_2 solutions of **3**-(*S*)mal (black trace) and silver(III)/silver(I) assembly **4** (red trace) obtained by transmetallation of **3**-(*S*)mal.

Data for **3**-Cl_2 crystals obtained from benzene solution: X-ray quality crystals of **3**-Cl_2 were obtained by slow diffusion of benzene solution of **3**-Cl_2 into heptane. Crystal data for **3**-Cl_2: $2(C_{96}H_{72}N_{16}Cl_2N_8Zn_2)\cdot C_7\cdot 2(H_2O)$ M_W = 3198.61, T = 100 K, CuK_α radiation, triclinic, space group P-1, a = 10.837(3), b = 23.325(6), c = 34.093(9) Å, α = 106.95(2), β = 95.93(2), γ = 101.13(2), V = 7971(4) Å^3, Z = 2, Dc = 1.333 Mg·m^{-3}, λ = 1.54178 Å, μ = 1.794 mm^{-1}, F(000) = 3316, diffractometer Oxford Diffraction Xcalibur PX with KM4CCD Sapphire detector, 3.86 ≤ θ ≤ 76.44°, 72868 collected reflections, 29037 independent reflections with $I > 2\sigma(I)$, 2025 parameters, $R_1(F)$ = 0.0656, $wR_2(F^2)$ = 0.1904, S = 1.002, largest difference peak and hole 1.031 and –0.397 e·Å^{-3}. All non-H atoms were refined with anisotropic displacement parameters except for those of the disordered solvent. Hydrogen atoms involved in the hydrogen bond formation were localized on the differential electron density map. The other hydrogen atoms were included from geometry of molecules and refined isotropically. The asymmetric unit contains two molecules of **3**-Cl_2 accompanied by two water molecules and one disordered heptane. Water molecules are involved in a network of hydrogen bonds between external nitrogen and axial chloride atoms. Selected parameters of these bonds are summarized in the table below.

D-H...A	D-H	H...A	D...A	<(DHA)
O1-H1S...Cl1	1.01(7)	2.26(7)	3.245(4)	167(6)
O2-H3S...Cl3	0.85(7)	2.39(7)	3.224(5)	169(7)
N26-H26...O1	0.80(6)	2.02(6)	2.820(5)	176(6)
N76-H76...O2	0.91(6)	1.95(6)	2.807(6)	158(5)

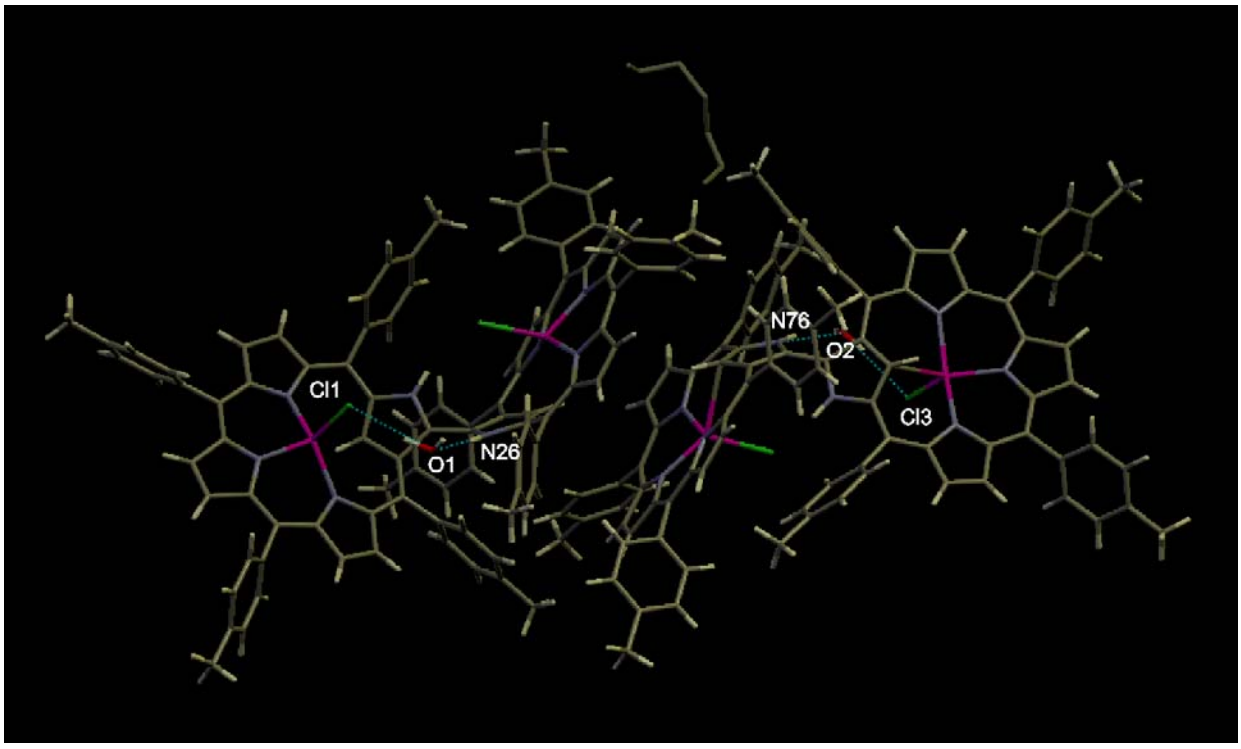

Fig. S18. A stick representation of the asymmetric unit of the **3**-Cl_2 crystal obtained from benzene solution with marked hydrogen bonds of the water within both symmetry-independent molecules of the dimer.

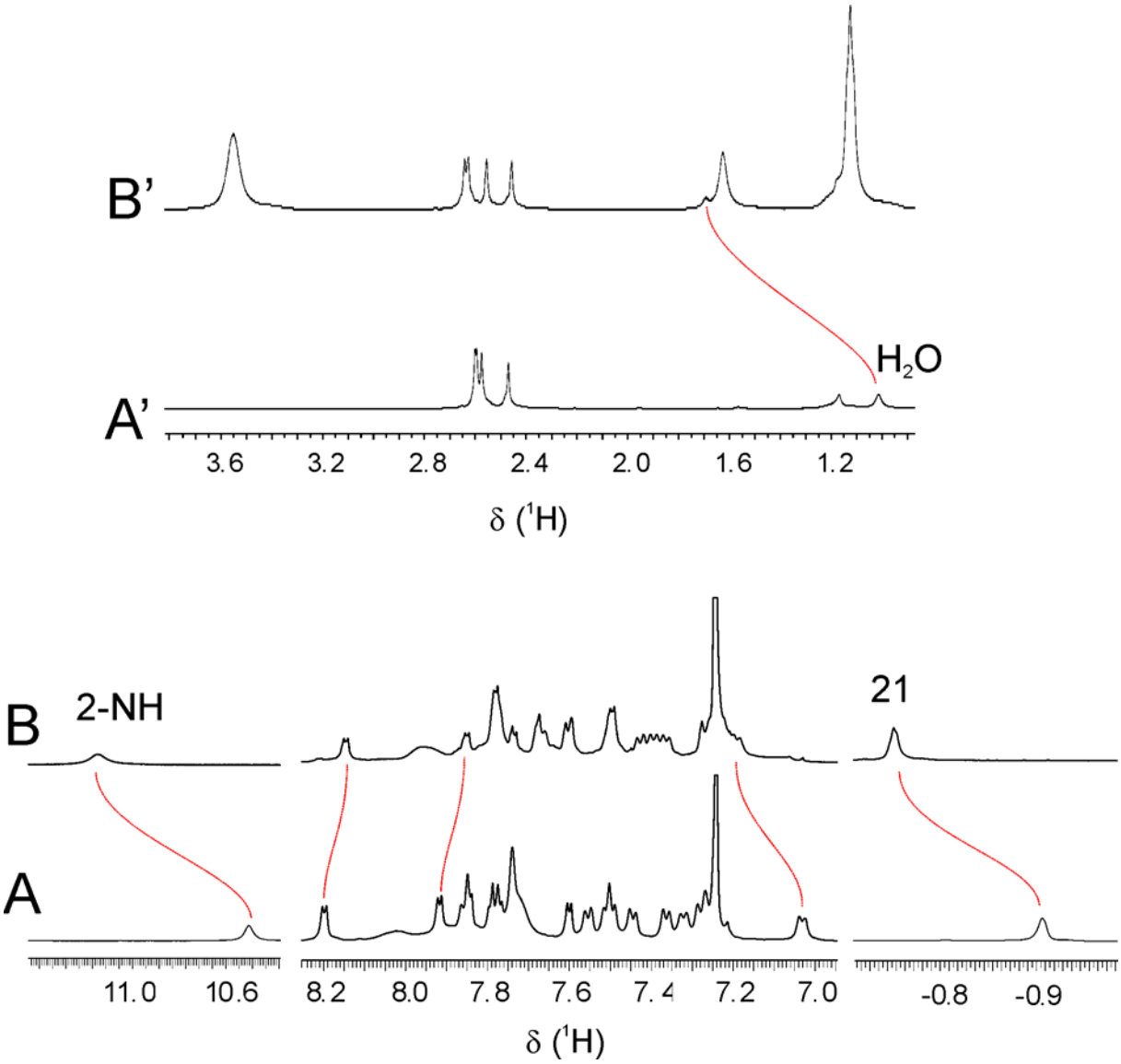

Fig. S19. ^{1}H NMR spectra of **3**-Cl_2 in $CDCl_3$ (A, A') and after addition of 30-fold excess of ethanol (B, B'). Both spectra recorded at 213 K.

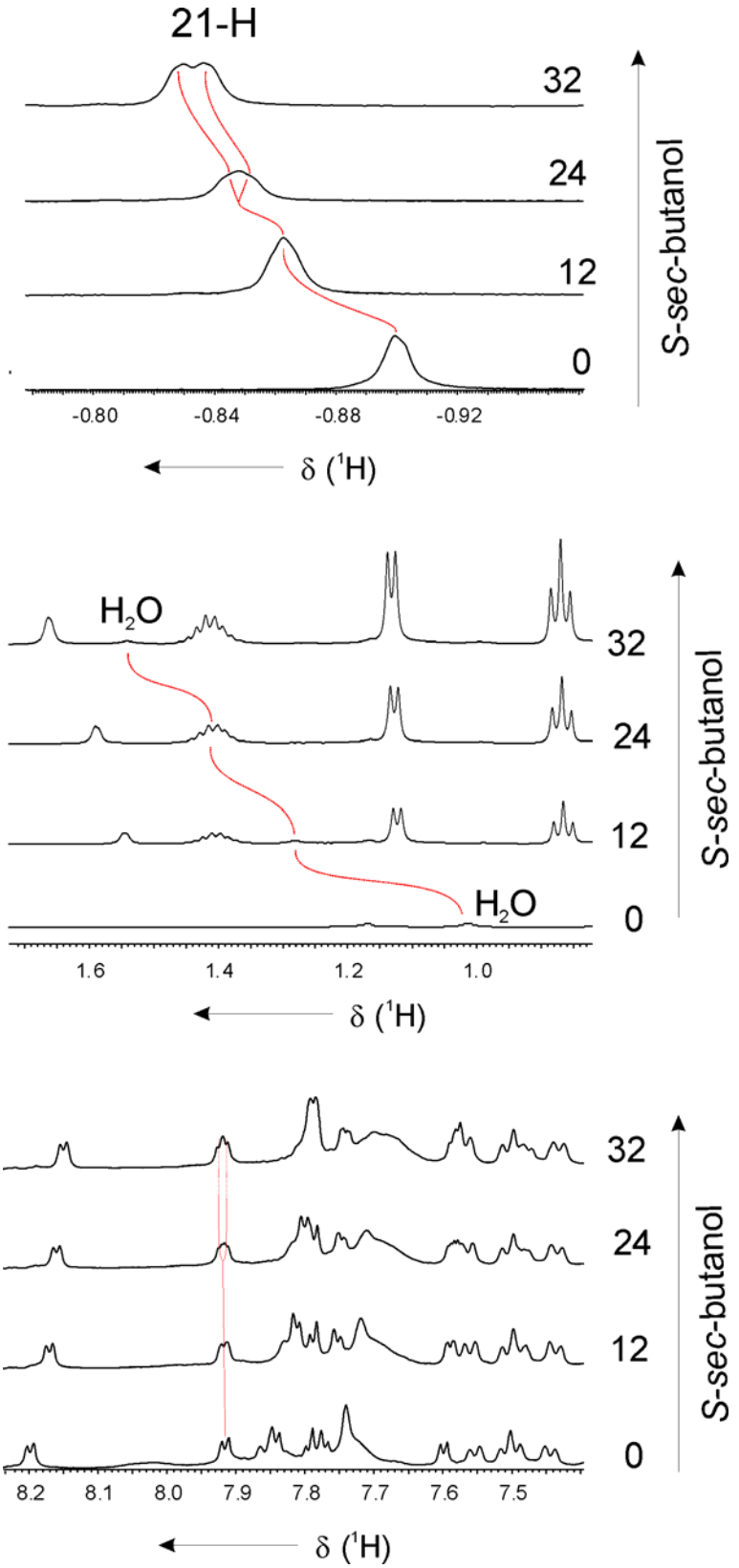

Fig. S20. Fragments of the ^{1}H NMR spectra of **3**-Cl_2 ($CDCl_3$, 213 K) recorded upon titration with (*S*)-*sec*-butanol. The molar excess of the alcohol is indicated on the right margin of each trace.

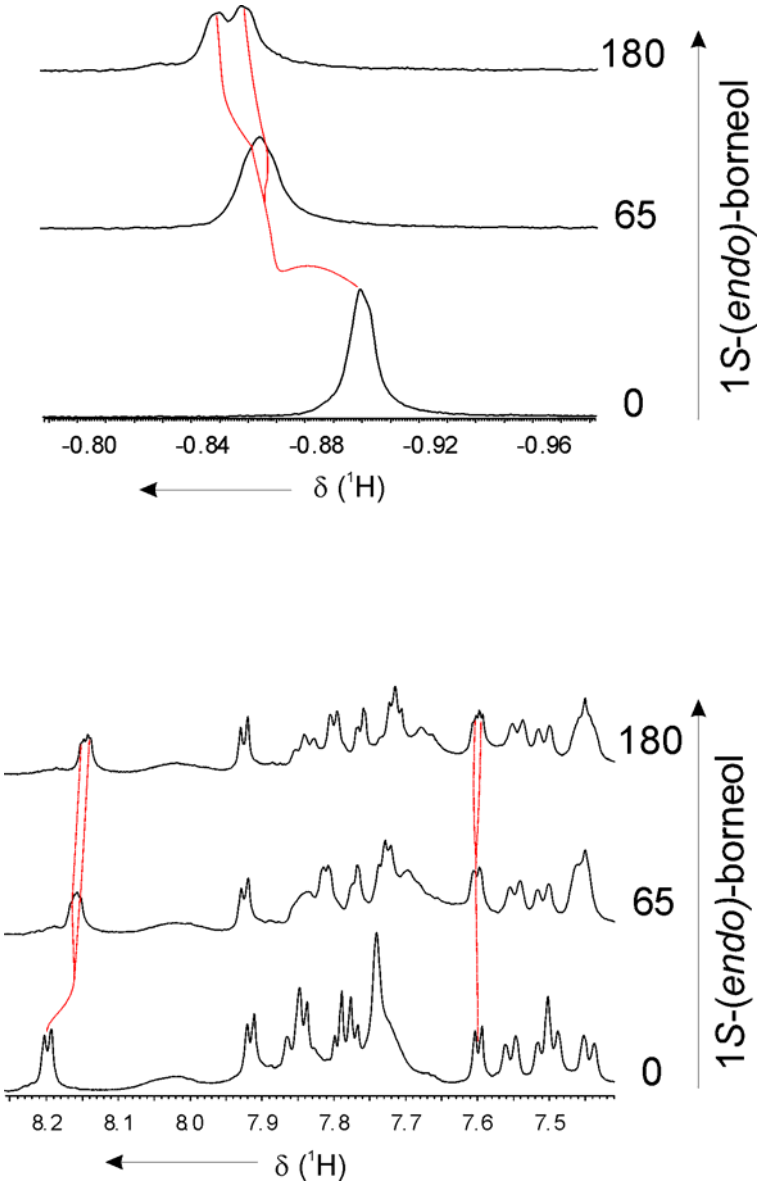

Fig. S21. Fragments of the ^{1}H NMR spectra of **3**-Cl_2 ($CDCl_3$, 213 K) recorded upon titration with (*S*)-(*endo*)-borneol. The molar excess of the alcohol is indicated on the right margin of each trace.

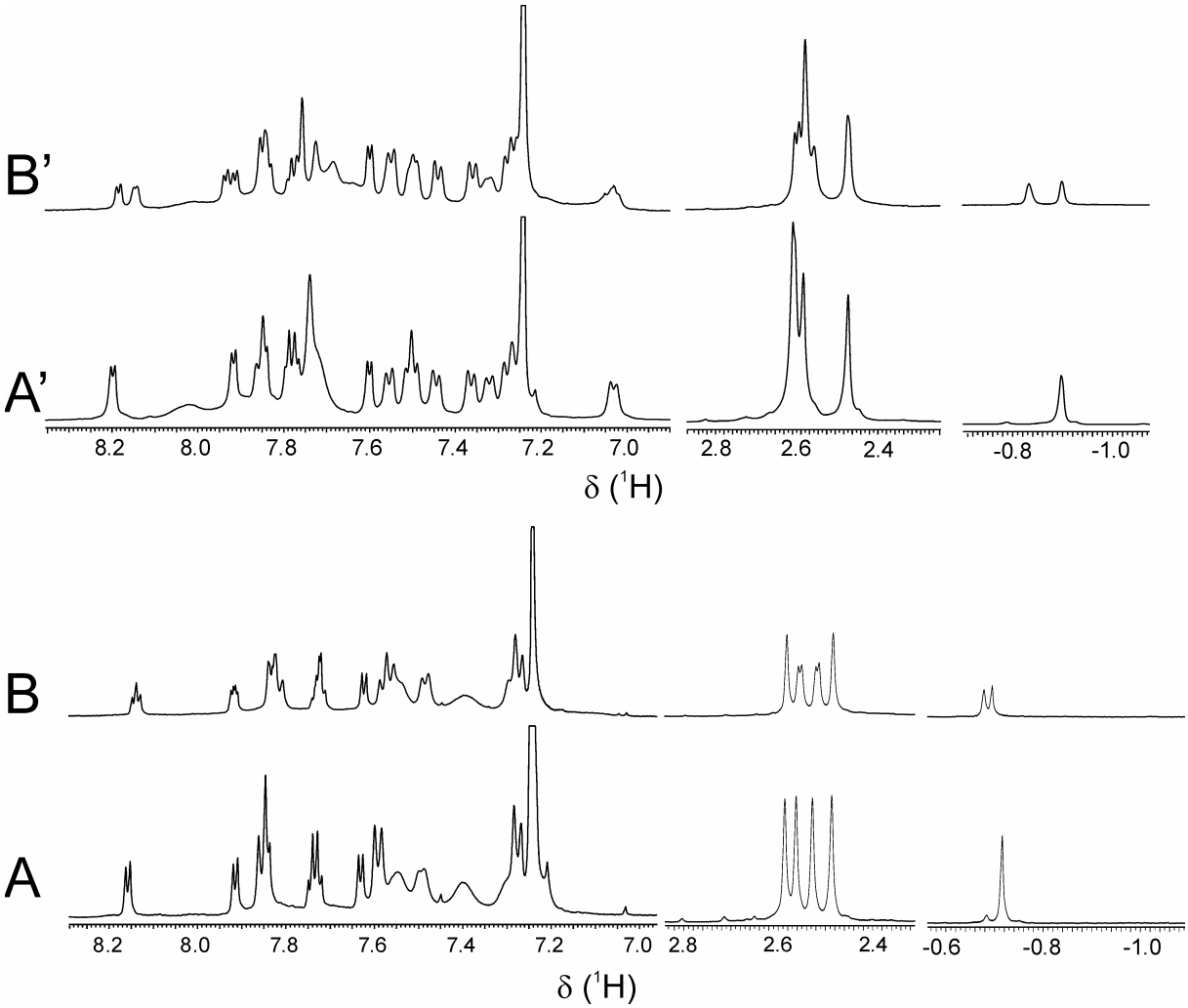

Fig. S22. Changes in ^{1}H NMR spectrum of 3-Cl_2 ($CDCl_3$, trace A, 298 K; trace A', 213 K) upon addition of 60 equivalents of (1*R*,2*S*,5*R*)-menthol (B, 298 K, B', 213 K).

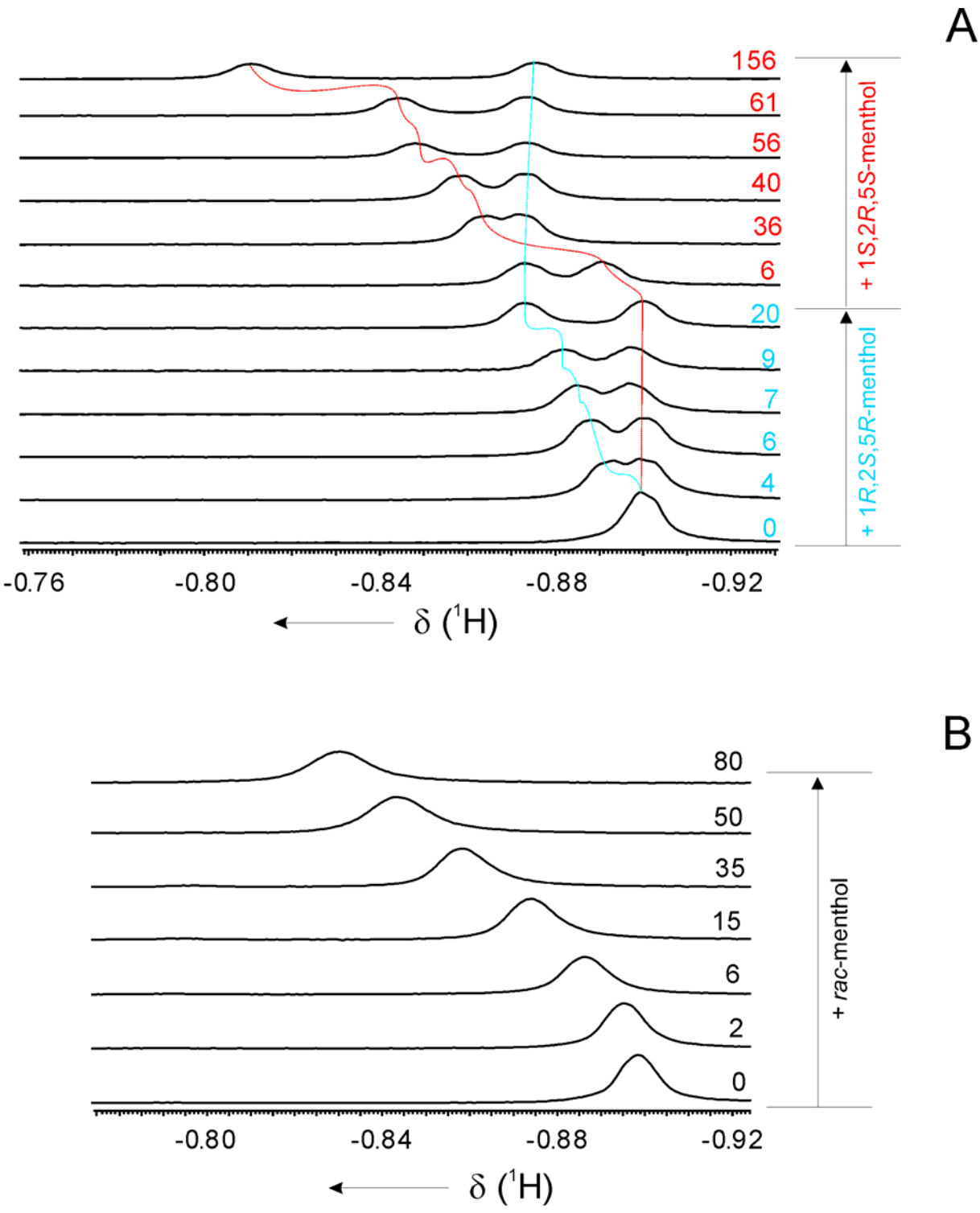

Fig. S23. High-field fragments of the ^{1}H NMR spectra of **3**-Cl_2 ($CDCl_3$, 213 K) recorded upon titration with indicated enantiomer of menthol (A; molar excess of each enantiomer with respect to the host is indicated on the right margin of each trace) or with racemic mixture of menthol (B).

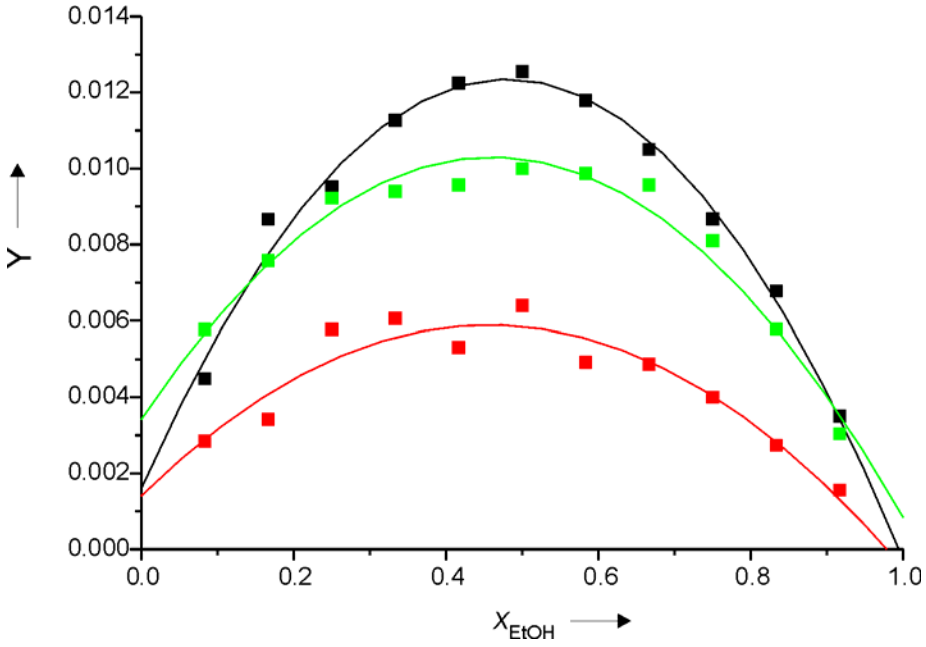

Fig. S24. Job plot for **3**-Cl_2 with ethanol at a total concentration of 1 mM in $CDCl_3$ at 213 K. The 21-CH (black), 7-CH (red), and 8-CH (green) protons of **3**-Cl_2 are reported; Y = (δ_{obs} – δ_0)*(molar fraction **3**-Cl_2), x_{EtOH} = molar fraction of ethanol.

Equimolar solutions (1 mM) of **3**-Cl_2 and ethanol in $CDCl_3$ were prepared and mixed in various ratios. In this way the total concentration of the components was kept constant at 1 mM and only the **3**-Cl_2/EtOH ratio was varied. ^{1}H NMR spectra of the mixtures were recorded, and the chemical shifts of **3**-Cl_2 were analyzed by Job's method of continuous variation. The maxima of the curves are at a mol fraction 0.5, confirming formation of the 1:1 adduct in solution. (M.T. Blanda, J. H. Horner, M. Newcomb, *J. Org. Chem.*, **1989**, *54*, 4626.)

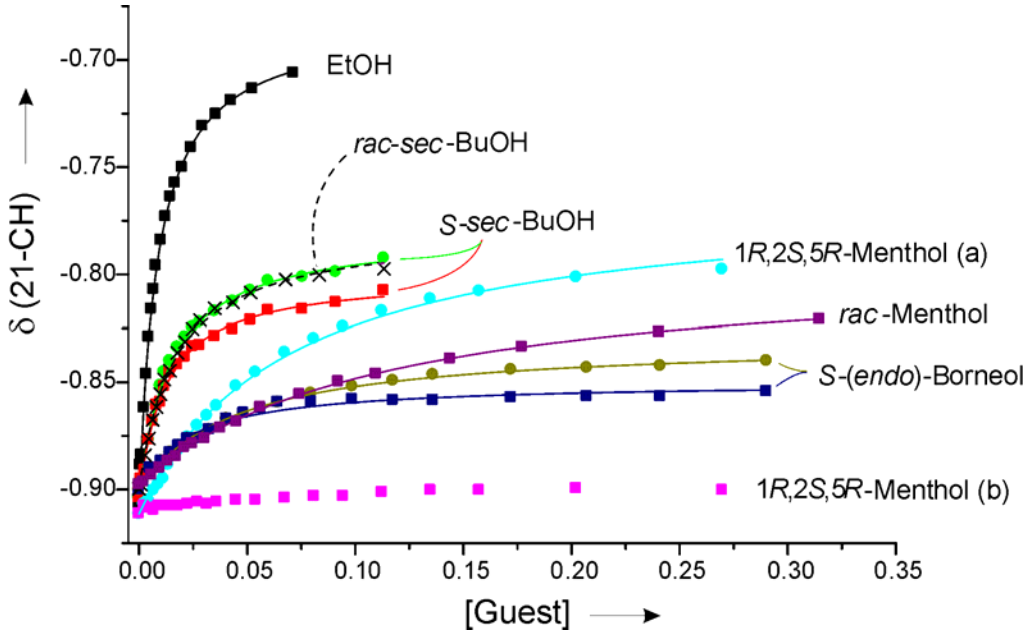

Fig. S25. Changes of chemical shift of 21-CH upon titration of **3**-Cl_2 with various alcohols specified near each trace. The theoretical curves are the best fit least-squares lines calculated on the basis of experimental points for the 1:1 adduct model. Formation of diastereomers causes splitting of the signal in the cases of enantiomerically pure chiral alcohols.

The ^{1}H NMR titrations of **3**-Cl_2 with various alcohols were carried out in $CDCl_3$ at 213 K. The concentration of **3**-Cl_2 was kept constant in all samples (1.7 mM) whereas the concentrations of guests were varied. The chemical shifts of protons 7, 8, and 21 which are most sensitive to the changes of alcohol concentration, were followed and fitted to a 1:1 binding model using a least-square fitting procedure to the following equation

$$\delta = \delta_F + (\delta_C - \delta_F)K[G]/(1 + K[G])$$

where δ is an observed chemical shift at a given guest's concentration [G], δ_F is chemical shift of **3**-Cl_2 at [G] = 0, K is an association constant, and δ_C is chemical shift of the (ROH)-**3**-Cl_2 adduct. The two latter parameters were optimized. The equation was derived assuming fast exchange between **3**-Cl_2 and (ROH)-**3**-Cl_2. Under such conditions $\delta = \delta_F x_F + \delta_C x_C$, where x_F and x_C are molar ratios of **3**-Cl_2 and (ROH)-**3**-Cl_2 at a given [G], respectively.
The association constants K were calculated as the mean of the values obtained for the each of the followed signals of the host, weighted by the observed changes in chemical shift ($\delta_C - \delta_F$). The association constants are collected in the table below. For enatiopure chiral alcohols two values of K are reported owing to the formation of diastereomers.

Alcohol	K
Ethanol	99.6
(*S*)-*sec*-Butanol	61.0; 62.8
(*rac*)-*sec*-Butanol	58.2
(*S*)-(*endo*)-Borneol	18.4; 19.6
(1*R*,2*S*,5*R*)-Menthol	< 2; 14.5
rac-Menthol	7.3

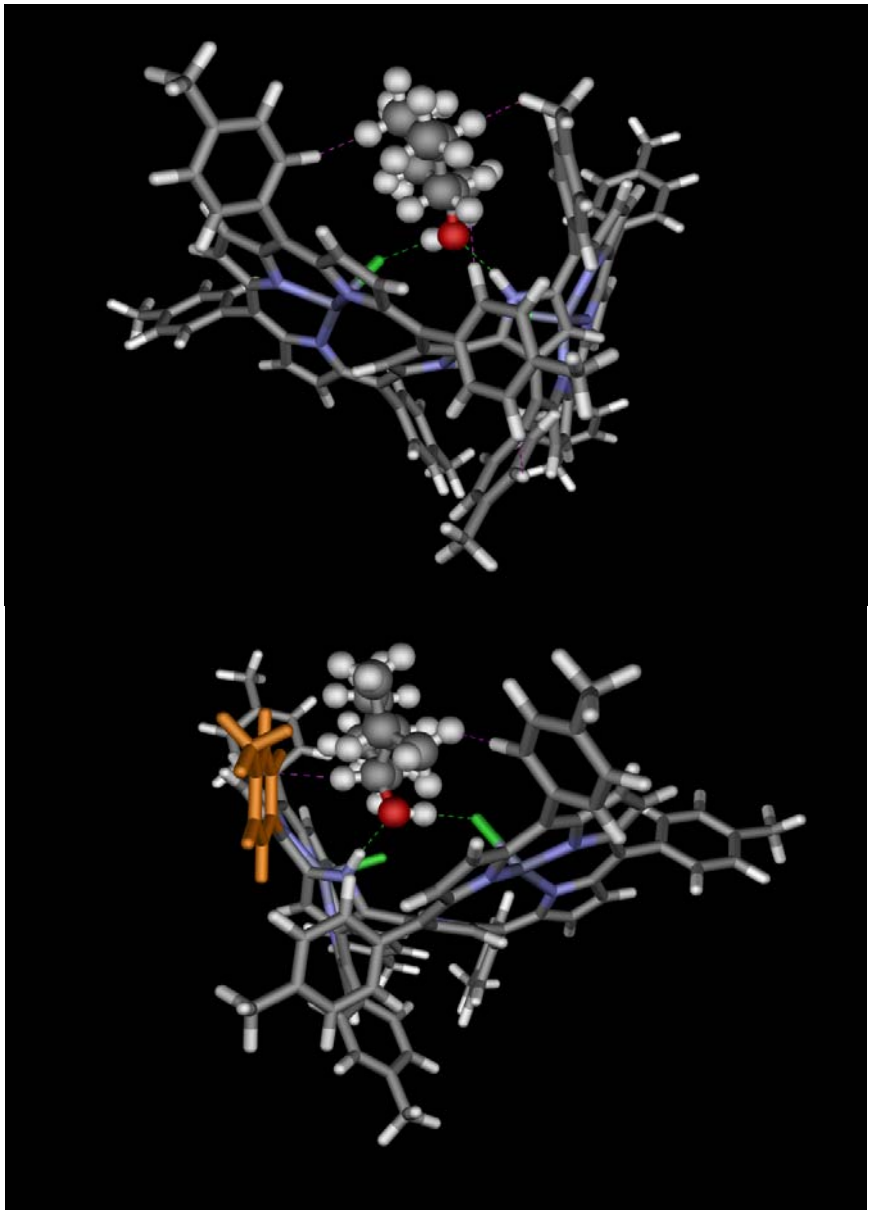

Fig. S26. The PM3 energy-optimized models of (1*R*,2*S*,5*R*)-menthol-(*P*)-**3**-Cl_2 (top) and (1*R*,2*S*,5*R*)-menthol-(*M*)-**3**-Cl_2 (bottom). The green dashed lines reflects hydrogen bonds, while the purple dashed lines show "bumps", i.e. short distances between non-bonded atoms (<1.9 Å for H-H, <2.3 Å for H-C). The models were constructed on the basis of enantiomers taken from the X-ray structure of **3**-Cl_2 by replacing water molecule with menthol while the H-bond systems were preserved. No restraints of any kind were imposed prior the geometry optimization. The difference between total energies of the modeled diastereomeric adducts is less than 1 kcal/mol. However, a strain may be assigned to the orientation of the tolyl substituent in the *meso* position 20 of (1*R*,2*S*,5*R*)-menthol-(*M*)-**3**-Cl_2 (orange colored) for which torsion angle C1-C20-C_{ipso}-C_{ortho} is 39° (usual value for this angle is 48-66°) reflecting restriction of a rotational freedom of the aryl ring caused by repulsive interaction with guest molecule. A short contact between one ortho carbon of this substituent and hydrogen on C1 of menthol (2.25 Å) also reflects spatial overcrowding for this diastereomer.